Phase-field modeling droplet dynamics with soluble surfactants

Haihu Liu, Yonghao Zhang*

Department of Mechanical Engineering, University of Strathclyde, Glasgow G1 1XJ, UK

Abstract

Using lattice Boltzmann approach, a phase-field model is proposed for simulating droplet motion with soluble surfactants. The model can recover the Langmuir and Frumkin adsorption isotherms in equilibrium. From the equilibrium equation of state, we can determine the interfacial tension lowering scale according to the interface surfactant concentration. The model is able to capture short-time and long-time adsorption dynamics of surfactants. We apply the model to examine the effect of soluble surfactants on droplet deformation, breakup and coalescence. The increase of surfactant concentration and attractive lateral interaction can enhance droplet deformation, promote droplet breakup, and inhibit droplet coalescence. We also demonstrate that the Marangoni stresses can reduce the interface mobility and slow down the film drainage process, thus acting as an additional repulsive force to prevent the droplet coalescence.

Keywords:
Phase field model, lattice Boltzmann model, soluble surfactant, Marangoni stress, Frumkin adsorption, droplet breakup and coalescence

1. Introduction

Surfactants are interfacially active agents that play an important role in many industrial processes, ranging from crude oil recovery, manufacture of cosmetics and pharmaceutical products, to food processing [1]. More recently, surfactants have been widely used in microfluidic applications [2].

*Corresponding author.
Email address: yonghao.zhang@strath.ac.uk (Yonghao Zhang)

Commonly-used surfactants are the molecules with polar head groups appended to hydrophobic tails, which selectively adhere to fluid interfaces forming a buffer zone to reduce the system energy. In microfluidic systems, surfactants are often used to generate small droplets and make them kinetically stable as emulsions even though water-in-oil and oil-in-water emulsions are thermodynamically unstable [3]. Capillary effect usually plays a dominant role in microfluidic system, and the presence of surfactants at interface will greatly modify interfacial tension. Therefore, surfactants are expected to significantly alter droplet dynamical behavior in the microfluidic devices [4, 5, 6]. A number of recent theoretical or numerical studies have reported to identify the mechanisms of droplet deformation, breakup and coalescence in the presence of surfactants [7, 8, 9, 10, 11, 12, 13, 14].

Modelling interfacial dynamics with soluble surfactants in a multiphase system is a daunting task. The surfactant molecules will self-assemble into a monolayer at the oil/water interface, thereby lowering interfacial tension. When the bulk concentrations are below the critical micelle concentration (CMC) and the surfactant lateral interactions are not important, the Langmuir adsorption can describe the realistic equilibrium adsorption behavior of non-ionic surfactants [15]. When the surfactant lateral interactions cannot be neglected, the Frumkin adsorption is more appropriate. Both advection and diffusion are important for surfactant transport at the interface and in the bulk phases. Non-uniform surfactant concentration (mainly at the interface) creates non-uniform interfacial tension forces and Marangoni stresses in the fluid, which in turn affect the flowfield. Meanwhile, the flowfield will influence the surfactant distribution. The interaction between surfactants and flowfield is highly non-linear, which poses a computational challenge. Most previous numerical work [7, 16, 17, 18, 19, 12, 20, 21] on surfactants has utilized the sharp interface models with an equilibrium equation of state relating dynamic interfacial tension to local surfactant concentration. The sharp interface models are built upon the conservation laws at the macroscopic level for interfacial dynamics, which have been developed from the original model proposed by Stone and Leal [7]. The models have been successfully applied to simulate interfacial flows in an oil/water/surfactant system. However, these sharp interface models suffer from several drawbacks:(i) dynamic interfacial tension relies on an asserted equilibrium equation of state, which is also assumed to be valid beyond the equilibrium state; (ii) for interfacial flows with soluble surfactants, mass transfer between the interface and the bulk fluids requires an external boundary condition, which cannot uniquely arise from

the model itself; (iii) model extension for more complicated systems, such as ionic surfactant solutions, is not easy [22]; (iv) numerical stability becomes a problem for the flows with large topological changes, such as droplet breakup and coalescence.

In contrast to sharp interface model, phase-field method, which can resolve the interface structure via an appropriate free energy functional, has shown great potential to simulate the multiphase flow problems [23, 24, 25, 26, 27, 28, 29]. In a phase-field model, the free energy not only determines the equilibrium properties, but also strongly influences the dynamics of the multiphase system. The transport of physical quantities can be linked to the free energy by a generalized hydrodynamic theory [30]. Hence, the phase-field models have a firm physical basis for multiphase flows, which is contrast to the traditional computational fluid dynamics (CFD) methods, e.g. the volume-of-fluid, level-set and front-tracking methods. Although phase-field models have shown promise for computation of binary mixture with surfactants [31, 32, 33], significant effort is still required to improve the model for realistic oil/water/surfactant systems. Here, we will present a generalized phase-field model in a lattice Boltzmann (LB) framework to simulate the adsorption of surfactants at the interface and its effect on droplet dynamics.

2. Phase-field model for immiscible fluids containing surfactants

The ternary system we consider consists of a nonionic surfactant solute and two immiscible solvents, say, oil and water. We aim to develop an improved phase-field model that is able to capture both thermodynamic and hydrodynamic effects associated with surfactants in realistic ternary systems.

2.1. Free energy theory

The thermodynamics of a system is determined by its free energy functional. The Landau-Ginzburg free energy functional has been commonly used to describe a binary mixture [34]

$$\mathscr{F} = \int \mathrm{d}\vec{x} \left[-\frac{a}{2}\phi^2 + \frac{b}{4}\phi^4 + \frac{\kappa}{2}(\nabla\phi)^2 \right], \tag{1}$$

where $\phi = (\rho_o - \rho_w)/\rho$ represents the relative concentration of the local compositions. As we aim to deal with two immiscible fluids, and oil and water are most commonly used in microfluidic applications, we use oil and

water to represent two immiscible fluids here. $\rho = \rho_o + \rho_w$ is the total density, while ρ_o and ρ_w are the densities of oil and water phases respectively. The first two terms in Eq.(1) correspond to the bulk phase behaviour, with minima $\phi = \pm\phi_b = \pm\sqrt{a/b}$ for the oil and water respectively. The last term reflects the cost of sustaining the oil/water interface. Hereafter, the subscripts 'b' and '0' denote the bulk phases and interface, and the superscripts '+' and '-' represent the oil and water bulk phases respectively.

As surfactants favor to adhere to the oil/water interface and lower the interfacial tension, and the interfacial tension lowering scale depends on the local surfactant concentration. To account for the surfactant effect, additional terms are introduced to the original Landau-Ginzburg free energy functional. Laradji et al. [35] proposed the free energy functional in the form of

$$\mathscr{F} = \int \mathrm{d}\vec{x} \left[-\frac{a}{2}\phi^2 + \frac{b}{4}\phi^4 + \frac{\kappa}{2}(\nabla\phi)^2 + \frac{c}{2}\psi^2 + \frac{w}{2}\psi^2\phi^2 - \frac{d}{2}\psi(\nabla\phi)^2 \right], \quad (2)$$

where ψ is the surfactant local concentration in an oil/water/surfactant system. The term $\frac{c}{2}\psi^2$ prevents the surfactants from forming clusters. The local coupling term $\frac{w}{2}\psi^2\phi^2$ guarantees small local surfactant concentration in the bulk phases, which is introduced to numerically stablise diffuse interface model for microemulsions. The last nonlocal coupling term $-\frac{d}{2}\psi(\nabla\phi)^2$ accounts for the energetic preference of surfactants when they are absorbed at the oil/water interface, favoring the lowering of interfacial tension.

Theissen and Gompper [31] chose a slightly different form of free energy functional to study the dynamics of spontaneous emulsification, where the local coupling term is replaced by $\frac{w}{2}\psi\phi^2$ to deal with the same solubility of surfactant in the bulk phases. Recently, Furtado et al. [33] applied a simpler form of free energy functional to phenomenologically describe the surfactant effect. In contrast to Eq. (2), the local coupling term vanishes and κ is expressed as a function of ψ to relate the interfacial tension to the surfactant concentration. We have derived the equilibrium equation of state following the free energy functional presented by Theissen and Gompper [31] (the details are shown in Appendix A), i.e.

$$\sigma(\psi_0) = \frac{4\phi_b^2}{3\xi}(\kappa - d\psi_0), \quad (3)$$

where ξ is a parameter proportional to the interface thickness, which is given

by

$$\xi^2 = \frac{2(\kappa - d\psi_0)}{\phi_b^2(b - \frac{w^2}{2c})} = \frac{2[\kappa - d(\psi_b + \frac{\phi_b^2 w}{2c})]}{\phi_b^2(b - \frac{w^2}{2c})}. \tag{4}$$

We note that the condition $Ex = \frac{d}{w\xi^2} \ll 1$ should be satisfied to analytically obtain Eqs. (3) and (4). Obviously, the free energy model proposed by Theissen and Gompper [31] cannot exhibit realistic adsorption isotherms such as the Langmuir/Frumkin adsorption isotherms. Similarly, we can show that the models proposed by Laradji et al. [35] and Furtado et al. [33] fail to recover the Langmuir/Frumkin adsorption isotherms. As both Langmuir/Frumkin adsorption isotherms are well developed for adsorption of non-ionic surfactants under the equilibrium state with the bulk surfactant concentrations below the CMC. It is important for any realistic model to recover these adsorption isotherms under the thermodynamical equilibrium state.

Diamant and Andelman [22] developed a sharp interface free energy model to describe the surfactant adsorption at the interface between an aqueous solution and another fluid phase. They introduced the ideal entropy of mixing into the model and treated the bulk solution and the interface as two coupled subsystems. The model can lead to the Frumkin adsorption isotherm in thermodynamic equilibrium. However, hydrodynamics was not considered in their model, so it cannot be applied to simulate droplet dynamic behavior with soluble surfactants.

Recently, van der Sman and van der Graaf [32] developed a diffuse interface model for surfactant adsorption onto the interface of two immiscible fluids. The free energy functional is partly adapted from the sharp interface model of Diamant and Andelman [22]. The model couples the surfactant adsorption to hydrodynamics, which demonstrates promising potential for phase-field model to simulate droplet dynamics in the presence of surfactants. However, the model is restricted to the Langmuir adsorption with equal solubility of the surfactants in both bulk phases. Although the model showed that the interfacial tension lowering $\Delta\sigma$ is proportional to $k_B T \ln(1-\psi_0)$ due to surfactant adsorption onto the interface, the dependence of the proportionality factor on the parameters used in the model is still unclear. Finally, the model capability is required to be further examined and demonstrated by simulating droplet dynamics with large topology changes.

To describe a ternary system including nonionic surfactant solute, we propose to extend the free energy functional given by van der Sman and van

der Graaf [32] to incorporate additional functionalities, e.g. the Frumkin adsorption isotherm, different solubility of the surfactants. Therefore, our free energy functional becomes:

$$\begin{aligned}\mathscr{F} = \quad & \int \mathrm{d}\vec{x} \left\{ -\frac{a}{2}\phi^2 + \frac{b}{4}\phi^4 + \frac{\kappa}{2}(\nabla\phi)^2 + \frac{w}{2}\psi\phi^2 - \frac{d}{2}\psi(\nabla\phi)^2 \right. \\ & \left. + k_B T \left[\psi \ln \psi + (1-\psi)\ln(1-\psi)\right] - \frac{c}{2}\psi^2 - e\phi\psi + \rho T \ln \rho \right\}, \quad (5)\end{aligned}$$

where the term involving the Boltzmann constant k_B is the ideal entropy of mixing of surfactant and solvent (i.e. steric effects), and solute and solvent molecules are assumed to have the same size [36]. The term $-\frac{c}{2}\psi^2$ is the energy of lateral interaction between two adjacent surfactants, where $c > 0$ is assumed to express an overall attractive interaction [22]. Note that this term plays a different role here as it appears in Eq. (2). The value of c cannot be 0 in Eq. (2), whereas in Eq. (5) c can be 0 when the lateral interaction is absent. The asymmetric term proportional to e accounts for different solubility of surfactants in the oil and water phases. The final term does not affect the phase behavior, but it is required to enforce incompressibility of the fluid in lattice Boltzmann model [37]. A suitable choice, based on improving numerical stability and accuracy, is $T = 1/3$.

The chemical potentials μ_ϕ and μ_ψ can then be obtained via the variational derivatives of the free energy functional Eq. (5) with respect to ϕ and ψ:

$$\mu_\phi = \frac{\delta\mathscr{F}}{\delta\phi} = -a\phi + b\phi^3 - (\kappa - d\psi)\nabla^2\phi + d\nabla\phi\cdot\nabla\psi + w\phi\psi - e\psi, \quad (6)$$

$$\mu_\psi = \frac{\delta\mathscr{F}}{\delta\psi} = k_B T[\ln\psi - \ln(1-\psi)] - c\psi + \frac{w}{2}\phi^2 - \frac{d}{2}(\nabla\phi)^2 - e\phi. \quad (7)$$

Excess chemical potential gradients give rise to a thermodynamic force (per unit volume) that can be expressed as the divergence of pressure tensor from the Gibbs-Duhem equality:

$$\vec{f}_V = -\nabla\cdot\mathbf{P} = -\phi\nabla\mu_\phi - \psi\nabla\mu_\psi, \quad (8)$$

with the pressure tensor $\mathbf{P}$ given by

$$\mathbf{P} = p_0\mathbf{I} + (\kappa - d\psi)(\nabla\phi)(\nabla\phi)^{\mathrm{T}}, \quad (9)$$

where $\mathbf{I}$ is the second-order unit tensor, p_0 is the scalar part of the pressure tensor which can be calculated by the thermodynamic relation as [31]

$$p_0 = \rho\frac{\delta\mathscr{F}}{\delta\rho} + \phi\mu_\phi + \psi\mu_\psi - f(\rho, \phi, \nabla\phi, \psi). \tag{10}$$

Here, $f(\rho, \phi, \nabla\phi, \psi)$ is the free energy density, i.e. the integrand in Eq. (5). Using Eqs. (5) and (10), we can get

$$\begin{aligned} p_0 &= \rho T - \frac{a}{2}\phi^2 + \frac{3b}{4}\phi^4 - \frac{\kappa}{2}(\nabla\phi)^2 - k_B T\ln(1-\psi) - \frac{c}{2}\psi^2 \\ &\quad -(\kappa - d\psi)\phi\nabla^2\phi + d\phi\nabla\phi\cdot\nabla\psi + w\psi\phi^2 - e\phi\psi. \end{aligned} \tag{11}$$

2.2. Hydrodynamics

A dynamic multiphase system needs to be described by not only thermodynamics but also hydrodynamics. Local conservation of fluid mass and momentum leads to the Navier-Stokes equations for Newtonian fluids:

$$\partial_t\rho + \nabla\cdot(\rho\vec{u}) = 0, \tag{12}$$

$$\partial_t(\rho\vec{u}) + \nabla\cdot(\rho\vec{u}\vec{u}) = \nabla\cdot\left[\rho\nu(\nabla\vec{u} + (\nabla\vec{u})^{\mathrm{T}})\right] + \vec{f}_V, \tag{13}$$

which describe the time evolution of the hydrodynamic variables, i.e. the fluid density ρ and the fluid velocity $\vec{u}$. Here, $\nu = \eta/\rho$ is the kinematic viscosity and $\vec{f_V}$ is the thermodynamic force given by Eq. (8). In principle, this model can introduce a composition-dependent viscosity [24, 29].

The evolution of the solvent composition ϕ and the local concentration of surfactant solute ψ are described by the Cahn-Hilliard equations, where the diffusion of ϕ and ψ is driven by gradients of chemical potentials μ_ϕ and μ_ψ:

$$\partial_t\phi + \nabla\cdot(\phi\vec{u}) = \nabla\cdot(M_\phi\nabla\mu_\phi), \tag{14}$$

$$\partial_t\psi + \nabla\cdot(\psi\vec{u}) = \nabla\cdot(M_\psi\nabla\mu_\psi), \tag{15}$$

where M_ϕ and M_ψ are the respective mobilities of the two order parameters, which are taken to be constants. Following Eq. (15), the surfactant flux $\vec{j}_\psi$ can be written as

$$\vec{j}_\psi = -M_\psi\nabla\mu_\psi. \tag{16}$$

To obtain the surfactant diffusion coefficient D_ψ, we can rewrite Eq. (16) into

$$\vec{j}_\psi = -M_\psi\frac{\partial\mu_\psi}{\partial\psi}\nabla\psi = -M_\psi\left[\frac{k_B T}{\psi(1-\psi)} - c\right]\nabla\psi, \tag{17}$$

with $D_\psi = M_\psi \left[\frac{k_B T}{\psi_b(1-\psi_b)} - c\right]$ in the bulk phases. Here, ψ_b is the surfactant concentration in the bulk phase. Once D_ψ is defined, Eq. (15) can recover the usual convection-diffusion equation

$$\partial_t \psi + \nabla \cdot (\psi \vec{u}) = \nabla \cdot (D_\psi \nabla \psi), \tag{18}$$

which has been widely used for bulk surfactant transport in the sharp interface model [38, 21, 14].

Similarly, the diffusivity of the interface can be defined as

$$D_\phi = M_\phi a(3\phi^2 - 1 + w\psi) \approx -M_\phi a, \tag{19}$$

with $\phi \approx 0$ and $w\psi \ll 1$ near the interface, as the relevant diffusion only takes place at the phase interface. Note that this "negative diffusion" maintains the solvent composition jump across the interface.

2.3. Thermodynamic equilibrium

In equilibrium, the thermodynamic force $\vec{f}_V$ becomes zero, and thereby the chemical potentials are equal throughout the entire system. We analyze whether the model can predict the equilibrium properties of the surfactant adsorption in oil/water solvents as described by the Langmuir and Frumkin isotherms. In a dilute solution, the bulk surfactant concentration is much smaller than unity, i.e. $\psi_b \ll 1$. We assume that the solvent composition profile is independent of the surfactant loading in equilibrium, which can be represented as

$$\phi(x) = \phi_b \tanh\left(\frac{x}{\xi}\right), \tag{20}$$

where ξ is a measure of the interface thickness as described by Eq. (A.14).

From Eq. (7), we can obtain the chemical potentials $\mu^+_{\psi,b}$ and $\mu^-_{\psi,b}$ in the oil and water bulk phases respectively:

$$\mu^+_{\psi,b} \approx k_B T \ln \psi^+_b + \frac{1}{2} w \phi_b^2 - e\phi_b, \tag{21}$$

$$\mu^-_{\psi,b} \approx k_B T \ln \psi^-_b + \frac{1}{2} w \phi_b^2 + e\phi_b, \tag{22}$$

where the magnitude of c is up to $\mathcal{O}(k_B T)$ [22]. The chemical potential at the interface is:

$$\mu_{\psi,0} = k_B T[\ln \psi_0 - \ln(1-\psi_0)] - c\psi_0 - \frac{d}{2\xi^2}\phi_b^2, \tag{23}$$

where we have used $\partial_x\phi = \phi_b/\xi$ at the interface $x = 0$ following Eq. (20).

In equilibrium, we have $\mu^+_{\psi,b} = \mu^-_{\psi,b} = \mu_{\psi,0}$. So from Eqs. (21), (22) and (23) for the chemical potentials, we can obtain the surfactant concentration ratio β in the oil and water bulk phases

$$\beta = \frac{\psi^+_b}{\psi^-_b} = \mathrm{e}^{\frac{2e\phi_b}{k_BT}}, \tag{24}$$

and the equilibrium adsorption isotherm

$$\psi_0 = \frac{\psi^\pm_b}{\psi^\pm_b + \psi^\pm_c \mathrm{e}^{-\frac{c}{k_BT}\psi_0}}, \tag{25}$$

with

$$\psi^\pm_c = \exp\left\{-\frac{1}{2k_BT}\left(\frac{d}{\xi^2} + w\right)\phi_b^2 \pm \frac{e}{k_BT}\phi_b\right\}. \tag{26}$$

Therefore, the model can recover the Frumkin adsorption isotherm (see Eq. (25)), which reduces to the well-known Langmuir adsorption isotherm if $c = 0$. Also, it can be clearly seen from Eq. (24) that we can use the parameter e to control the solubility of surfactant in oil-rich phase and water-rich phase. For the sake of simplicity, we assume the same solubility of surfactant in both phases, i.e. $e = 0$, in the following analysis.

In Appendix A, the equilibrium solvent composition profile is analytically demonstrated to be independent of the surfactant loading. With the solvent composition profile ϕ given by Eq. (20), we can obtain an analytical expression for the surfactant concentration at an arbitrary position x from Eq. (7):

$$\psi(x) = \frac{1}{1 + \mathrm{e}^{-\frac{1}{k_BT}\left[\mu_\psi - \frac{w}{2}\phi^2 + \frac{d}{2}(\partial_x\phi)^2\right]}\mathrm{e}^{-\frac{c}{k_BT}\psi}}, \tag{27}$$

where μ_ψ is determined by Eq. (21) or Eq. (22).

In the sharp interface models, the equilibrium equation of state can be derived via integration of the Gibbs equation:

$$\mathrm{d}\sigma = -\psi_0 \mathrm{d}\mu_\psi. \tag{28}$$

For the diffuse interface model, the excess surfactant concentration has to be obtained by the integration over the whole diffuse interface [39], and thus the equilibrium equation of state cannot be analytically obtained. Following van

der Sman and van der Graaf [32], we also assume that the excess surfactant concentration is proportional to ψ_0, so that the interfacial tension lowering is proportional to that of the sharp interface with a coefficient α, i.e.

$$\mathrm{d}\sigma = -\alpha\psi_0 \mathrm{d}\mu_{\psi,0}. \tag{29}$$

Substituting Eq. (23) into Eq. (29), we can obtain the equilibrium equation of state:

$$\Delta\sigma = \sigma - \sigma_0 = \alpha[k_B T \ln(1-\psi_0) + \frac{c}{2}\psi_0^2], \tag{30}$$

where $\sigma_0 = 4\kappa\phi_b^2/3\xi$ is the interfacial tension of "clean" droplet i.e. $\psi = 0$. We find that the coefficient α is a model-dependent constant in Eq. (30). In the sharp interface model, $\alpha = 1$, whereas in the diffuse interface model, $\alpha \neq 1$, due to the finite interface thickness. Therefore, α should depend on the excess of surfactant, while it is independent of ψ_0 and c/k_BT. For the given values of ψ_c and β, the excess surfactant concentration ψ_{ex} is a function of Ex, ψ_0 and ξ. As α is independent of ψ_0, α only depends on $Ex = \frac{d}{w\xi^2}$ once ξ is specified. Note, unlike the widely-used sharp interface model proposed by Stone and Leal [7], the phase-field method can also describe non-equilibrium effect of surfactant adsorption.

3. Lattice Boltzmann method

Lattice Boltzmann (LB) method has been widely used by researchers [40, 41, 42, 43] to model multiphase flows. As a pseudo-molecular method, it solves a discretized version of the Boltzmann equation to track evolution of the distribution function of an assembly of molecules [44]. Here, we will use LB method to simulate multiphase flows described by Eqs. (12)-(15). For a ternary fluid, we define three particle distribution functions f_i, g_i and h_i on each site of a two-dimensional square lattice with spacing δ_x. The subscript i denotes a particular lattice velocity vector $\vec{e}_i$, defined by $\vec{e}_0 = (0,0)$, $\vec{e}_{1,3} = (\pm c, 0)$, $\vec{e}_{2,4} = (0, \pm c)$, $\vec{e}_{5,7} = (\pm c, \pm c)$ and $\vec{e}_{6,8} = (\mp c, \pm c)$. The lattice velocity parameter c is defined as $c = \delta_x/\delta_t$ with δ_t being the simulation time step.

The macroscopic physical variables are obtained as moments of the particle distribution functions

$$\begin{aligned} \phi = \sum_i g_i, \quad \psi = \sum_i h_i, \\ \rho = \sum_i f_i, \quad \rho\vec{u} = \sum_i f_i \vec{e}_i. \end{aligned} \tag{31}$$

The time evolution equation for the particle distribution functions, using the standard Bhatnagar-Gross-Krook (BGK) approximation, can be written as

$$f_i(\vec{x}+\vec{e}_i\delta_t, t+\delta_t) - f_i(\vec{x},t) = \frac{1}{\tau_f}[f_i^{eq}(\vec{x},t) - f_i(\vec{x},t)], \tag{32}$$

$$g_i(\vec{x}+\vec{e}_i\delta_t, t+\delta_t) - g_i(\vec{x},t) = \frac{1}{\tau_g}[g_i^{eq}(\vec{x},t) - g_i(\vec{x},t)], \tag{33}$$

$$h_i(\vec{x}+\vec{e}_i\delta_t, t+\delta_t) - h_i(\vec{x},t) = \frac{1}{\tau_h}[h_i^{eq}(\vec{x},t) - h_i(\vec{x},t)], \tag{34}$$

where τ_f, τ_g and τ_h are independent scalar relaxation parameters, and f_i^{eq}, g_i^{eq} and h_i^{eq} are the equilibrium distribution functions for each distribution function.

The equilibrium distribution functions satisfy the conditions of mass and momentum conservation, as well as the additional constraints with the higher order moments:

$$\begin{aligned}
&\sum_i f_i^{eq} = \rho, \quad \sum_i g_i^{eq} = \phi, \quad \sum_i h_i^{eq} = \psi, \\
&\sum_i f_i^{eq}\vec{e}_i = \rho\vec{u}, \quad \sum_i g_i^{eq}\vec{e}_i = \phi\vec{u}, \quad \sum_i h_i^{eq}\vec{e}_i = \psi\vec{u}, \\
&\sum_i f_i^{eq}\vec{e}_i\vec{e}_i^{\mathrm{T}} = \mathbf{P} + \rho\vec{u}\vec{u}^{\mathrm{T}}, \\
&\sum_i g_i^{eq}\vec{e}_i\vec{e}_i^{\mathrm{T}} = \Gamma_\phi\mu_\phi\mathbf{I} + \phi\vec{u}\vec{u}^{\mathrm{T}}, \\
&\sum_i h_i^{eq}\vec{e}_i\vec{e}_i^{\mathrm{T}} = \Gamma_\psi\mu_\psi\mathbf{I} + \psi\vec{u}\vec{u}^{\mathrm{T}}.
\end{aligned} \tag{35}$$

Therefore, the dynamics of system is governed by the appropriate set of continuum equations. Explicit expressions for f_i^{eq}, g_i^{eq} and h_i^{eq} are given in Appendix B.

Using the Chapman-Enskog expansion, the lattice Boltzmann model Eqs.(32)-(34) can lead to Eqs. (12)-(15) in the long-wavelength and low-frequency limit. The relaxation parameters τ_f, τ_g and τ_h are related to the kinematic viscosity and mobilities through

$$\nu = c_s^2(\tau_f - 1/2)\delta_t, \tag{36}$$

$$M_\phi = \Gamma_\phi(\tau_g - 1/2)\delta_t, \quad M_\psi = \Gamma_\psi(\tau_h - 1/2)\delta_t, \tag{37}$$

where c_s is the speed of sound which is $c/\sqrt{3}$. Note that we set $\tau_g = \tau_h = 1/(3-\sqrt{3})$ to minimize numerical errors of the convection-diffusion scheme [45]. So Γ_ϕ (Γ_ψ) can act as a tunable parameter to control M_ϕ (M_ψ).

In our lattice Boltzmann multiphase model, the calculations of gradient and Laplacian operators are required to evaluate the chemical potentials in Eqs. (6) and (7) as well as the pressure tensor in Eq. (9). To minimize the discretization error, these operators are calculated using 9-point finite difference stencils as follows:

$$\begin{aligned} \nabla\phi(\vec{x}) &= \frac{1}{c_s^2\delta_t}\sum_i w_i\phi(\vec{x}+\vec{e}_i\delta_t)\vec{e}_i, \\ \nabla^2\phi(\vec{x}) &= \frac{2}{c_s^2\delta_t^2}\sum_i w_i[\phi(\vec{x}+\vec{e}_i\delta_t)-\phi(\vec{x})], \end{aligned} \tag{38}$$

where w_i is the weight factor with $w_0 = 4/9$, $w_{1-4} = 1/9$ and $w_{5-8} = 1/36$.

4. Model validation and applications

4.1. Equilibrium properties

First, we will numerically test the present phase-field model's capability for prediction of the profile of surfactant concentration at a planar oil-water interface. The flow domain contains 202×4 square lattices in the xy-plane with an oil phase initially located at $51 \le x \le 150$. The periodic boundary conditions are imposed at all the boundaries. We run our simulations with these parameters: $\sigma_0 = 0.02$, $\xi/\delta_x = 3$, $\psi_c = 0.017$, $Ex = 0.17$, $d = \kappa$, $M_\phi = 0.2$, $M_\psi = 0.02$, $\psi_b = \{10^{-4}, 10^{-3}, 5\times10^{-3}\}$, $c = 0$ for the Langmuir adsorption, and $2k_BT$ for the Frumkin adsorption.

Fig. 1 (a) shows excellent agreement between our numerical results and the analytical solution given by Eq. (27). For the two different adsorption isotherms, the profiles of surfactant concentration exhibit a large difference only when the value of ψ_0 is large. As seen in Fig. 1 (b), the predicted solvent composition profile $\phi(x)$ agrees well with the analytical solution, $\phi(x) = \phi_b \tanh(x/\xi)$, in all the cases. Therefore, the results confirm that the solvent composition profile is independent of the surfactant loading, which is assumed in obtaining our analytical solution. However, our numerical prediction will deviate from the analytical solution when ψ_0 is sufficiently large, which may attribute to two factors. The first one is that we cannot obtain Eq. (A.13) with χ approximated by $k_BT(\frac{1}{\psi_b} + \frac{1}{1-\psi_b}) - c$ due to the large surfactant

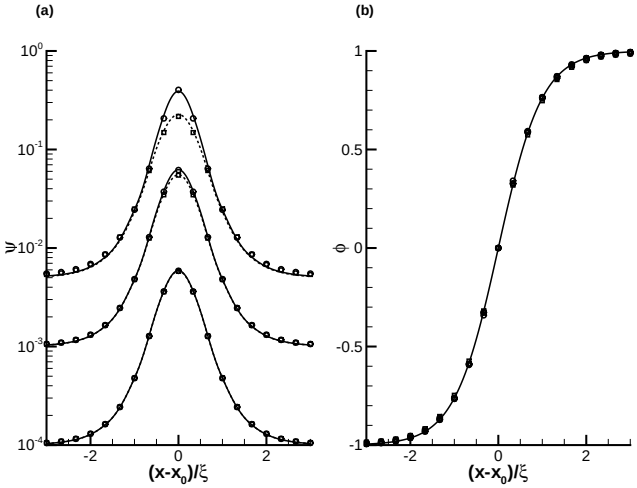

Figure 1: (a) Profile of the surfactant concentration for a planar oil-water interface located at $x_0 = 50$ (or $x_0 = 151$) with various parameters listed in the text. Square and circle symbols represent numerical predictions for $c = 0$ and $c = 2k_BT$ respectively, and the dashed and solid lines are the corresponding analytical solutions. (b) Profile of the solvent composition ϕ: the square symbols and circle symbols represent numerical predictions corresponding to $c = 0$ and $c = 2k_BT$ respectively; the solid line is the analytical solution of $\phi(x) = \phi_b \tanh(x/\xi)$.

excess at the interface, whereas the analytical solution Eq. (27) is derived on the basis of the parameter of the interface thickness satisfying $\xi^2 = \frac{2\kappa}{b\phi_b^2}$. Consequently, the predicted solvent composition profile cannot follow $\phi(x) = \phi_b \tanh(x/\xi)$ with $\xi = 3\delta_x$ as in the present simulation. The other factor may be due to the discretization error for the approximation of $\nabla\psi$, which increases rapidly as ψ_0 becomes large. We have also examined the influence of parameter ξ on the simulation results, which is shown in Fig. 2 for $\xi = \delta_x$ and $\xi = 2\delta_x$. It suggests that $\xi = 2\delta_x$ is still acceptable but $\xi = \delta_x$ is not a good choice. To correctly capture the sharp profile of surfactant concentration across the interface, a reasonably thick interface ($\xi \geq 2\delta_x$) is important. Considering the numerical accuracy, we choose $\xi \geq 2\delta_x$ in the following simulations.

Understanding the interfacial tension modification due to the presence of surfactants is practically important. Here, we will perform numerical simulations in a 121×121 domain with a droplet whose radius R is 30 lattices centred in the middle of the flow domain. We choose $d = \kappa$, $\psi_c = 0.017$, $\xi/\delta_x = 2$, $M_\phi = 0.1$, $M_\psi = 0.02$, and different values for σ_0, Ex, c and ψ_b. The profiles of ϕ and ψ are initialized with the analytical solutions given by Eqs. (20) and (27). When the droplet reaches its equilibrium, we calculate the interfacial tension σ by the Laplace law:

$$\Delta p = \frac{\sigma}{R}, \tag{39}$$

where Δp is the pressure difference across the droplet interface with the pressure p defined by $p = \frac{1}{2}P_{\alpha\alpha}$.

Eq. (30) shows the relation between the lowering of the interfacial tension $\Delta\sigma$ and the surfactant concentration at the interface. To validate this equilibrium relation, seven numerical simulation cases are performed with the following parameters: 1) $\sigma_0 = 0.02$, $Ex = 2$ and $c = 0$, 2) $\sigma_0 = 0.02$, $Ex = 1$ and $c = 0$, 3) $\sigma_0 = 0.01$, $Ex = 0.5$ and $c = 0$, 4) $\sigma_0 = 0.01$, $Ex = 0.5$ and $c = 2k_BT$, 5) $\sigma_0 = 0.01$, $Ex = 0.25$ and $c = 0$, 6) $\sigma_0 = 0.01$, $Ex = 0.25$ and $c = 2k_BT$, 7) $\sigma_0 = 0.01$, $Ex = 0.25$ and $c = 3k_BT$. In Fig. 3, we plot $\Delta\sigma/\sigma_0$ as a function of ψ_0, where the coefficient α in Eq. (30) is determined by the best fitting of our simulation results. In all these cases, it can be observed that the lowering of the interfacial tension follows the equation of state given by Eq. (30) when ψ_0 is not large ($\psi_0 < 0.5$). As we expect, the coefficient α is only dependent on Ex. Specifically, when $Ex = \{0.25, 0.5, 1.0, 2.0\}$, the corresponding values of α are $\{2.0, 2.2, 2.4, 2.8\}$. For a large ψ_0, our simula-

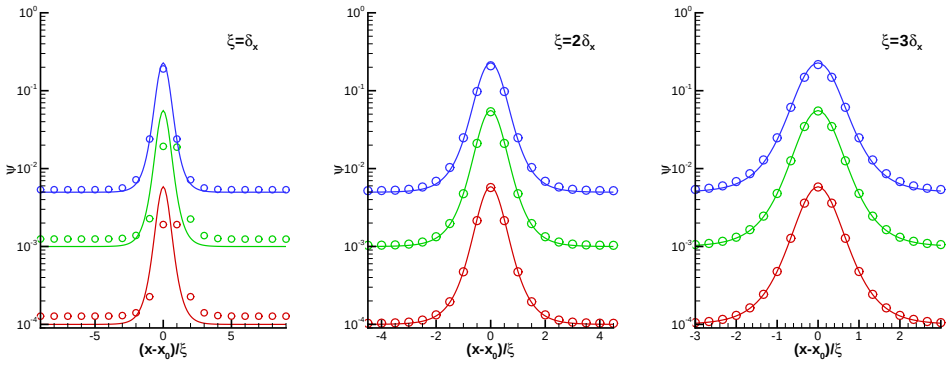

(a)

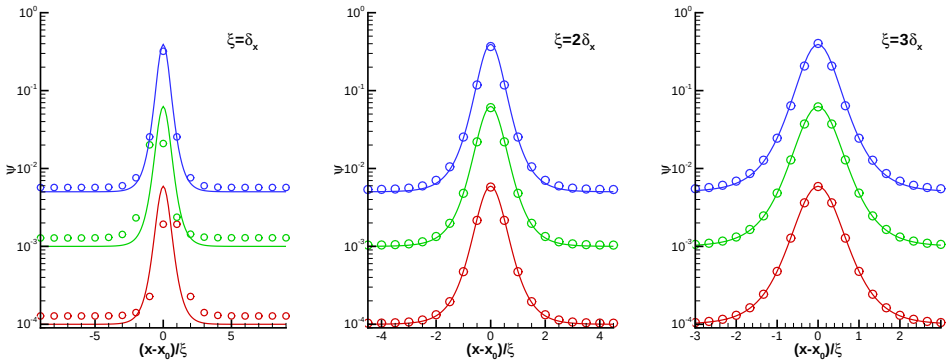

(b)

Figure 2: The effect of ξ on the profile of the surfactant concentration: (a) $c = 0$; (b) $c = 2k_BT$. Simulation results are represented by the discrete symbols, and the solid lines are the analytical solutions.

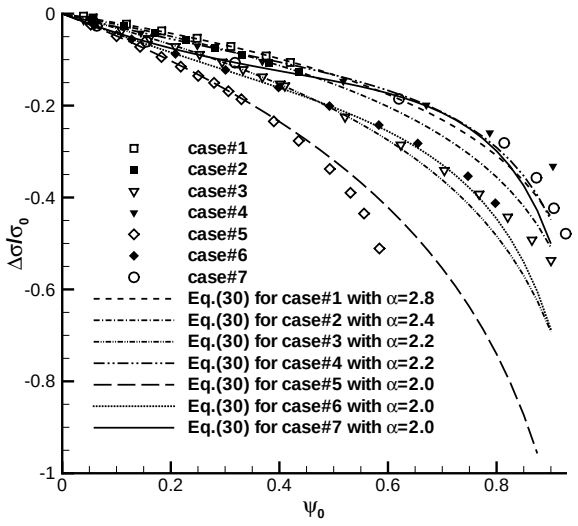

Figure 3: The lowering of interfacial tension $\Delta\sigma/\sigma_0$ as a function of the surfactant concentration at the interface ψ_0. The parameters are described in the text. Simulation results are indicated by the discrete symbols, and the lines are the solutions of Eq. (30) with the coefficient α determined by the best fitting of the simulation data.

tion results deviate from the analytical solutions of Eq. (30), which is also caused by the two factors as discussed in Fig. 1. Nevertheless, the intrinsic dependence of $\Delta\sigma$ on ψ_0 still holds.

A numerical artifact observed in many numerical methods is the existence of spurious velocities at the phase interface. Based on the analysis of the flowfield for a clean droplet in quiescent fluid, van der Sman and van der Graaf [27] have shown that the magnitude of the spurious velocities is proportional to the interfacial tension. It is interesting to study the influence of the interfacial tension σ_0 and the surfactant concentration ψ_b on the spurious velocities. Fig. 4 shows the maximal spurious velocities as a function of σ_0 for different c and ψ_b at a fixed Ex which is 0.25. It can be clearly seen that the addition of surfactant can decrease the spurious velocities, and the large surfactant concentration leads to bigger reduction of spurious velocities. For the same c and ψ_b, the magnitude of spurious velocities is also proportional to σ_0, which is similar to the case of clean droplet. Additionally, a multiphase system is always evolving towards the direction of free energy

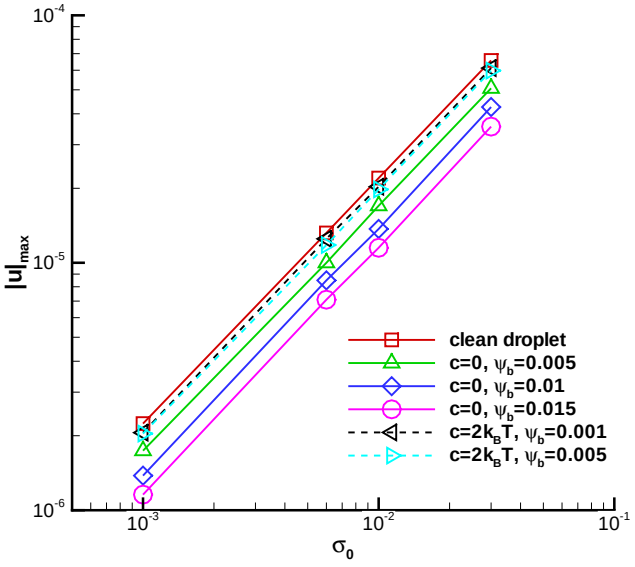

Figure 4: The maximal value of spurious velocities $|\vec{u}|$ as a function of σ_0 for both clean and contaminated droplets.

decreasing in phase field model. It has been found that small droplets are prone to dissolve in a surfactant-free finite system [27]. This is also observed in the surfactant-contaminated finite systems in our simulations. We also find that the addition of surfactants has negligible effect on dissolution of droplets.

4.2. Adsorption dynamics

Ward and Tordai [46] theoretically considered the adsorption dynamics of surfactant molecules from a semi-infinite bulk surfactant solution to an interface. The bulk phase and interface are assumed to have an initial surfactant concentration ψ_b and $\psi_0 = 0$ respectively. Surfactant molecules will diffuse from the bulk phase to the interface due to the concentration gradient. Consequently, the surfactant concentration at the interface will rise, while depleting the surfactants in the layer of fluid adjacent to the interface (termed as the subsurface). Soon, the interface is in local equilibrium with the subsurface, and the adsorption process slows down as the surfactant molecules have to transport over longer distances from the bulk phase to the

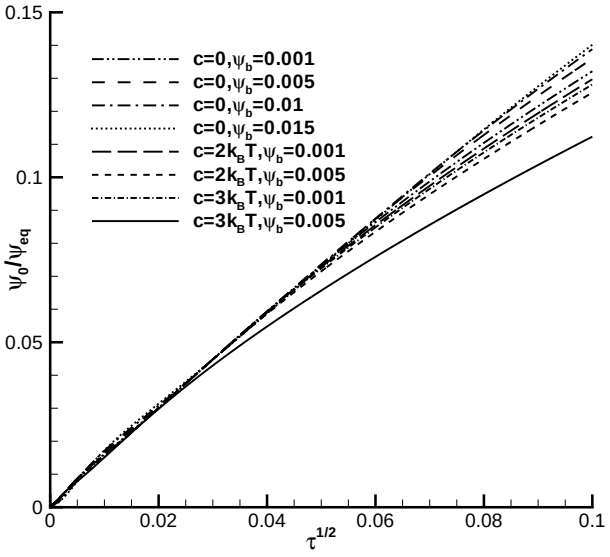

Figure 5: Short-time behavior of the surfactant concentration at the interface.

interface. The time-dependent adsorption process can be expressed by [46]

$$\psi_0(t) = 2\sqrt{\frac{D_\psi}{\pi}}\left[\psi_b\sqrt{t} - \int_0^{\sqrt{t}} \psi_s(u)\mathrm{d}\sqrt{t-u}\right], \tag{40}$$

where t is time, u is a dummy time-delay variable, and $\psi_s(u)$ is the surfactant concentration at the subsurface. We note that Eq. (40) is the analytical solution of the classical Ward and Tordai problem with the governing equation Eq. (18) in the sharp interface model, and it can be numerically solved with a given adsorption isotherm which relates the interface excess ψ_0 to ψ_s [47].

We apply the present phase-field model to investigate the Ward and Tordai problem, where an oil-water planar interface with an equal surfactant diffusion coefficient D_ψ in both bulk phases. We adopt the previously used definition of adsorption length $L_{ad} = \psi_{eq}/\psi_b$ [48, 49], where ψ_{eq} is determined by the adsorption isotherm:

$$\psi_{eq} = \frac{\psi_b}{\psi_b + \psi_c \mathrm{e}^{-\frac{c}{k_B T}\psi_{eq}}}. \tag{41}$$

And we choose the characteristic time as L_{ad}^2/D_ψ, so that the nondimensional time, τ, is tD_ψ/L_{ad}^2 [48, 49]. Therefore, the original dimensional Eq. (40), when cast into dimensionless form, becomes

$$\frac{\psi_0(\tau)}{\psi_{eq}} = \frac{2}{\sqrt{\pi}}\sqrt{\tau}, \tag{42}$$

for the short-time ($t \to 0$) adsorption behavior in the Ward and Tordai problem. This behavior is independent of the adsorption isotherm and the bulk surfactant concentration. The short-time adsorption behavior is examined using the model in a 401×4 lattices domain with the following parameters: $\psi_c = 0.017$, $Ex = 0.23$, $\xi/\delta_x = 3$ and $d = \kappa$. The Langmuir adsorption ($c = 0$) and Frumkin adsorption ($c/k_BT = \{2, 3\}$) are considered with $\psi_b = \{10^{-3}, 5 \times 10^{-3}, 10^{-3}, 1.5 \times 10^{-2}\}$ and $\psi_b = \{10^{-3}, 5 \times 10^{-3}\}$ respectively. Halfway bounce-back boundary conditions [50] are applied at $x = \pm 200$. The simulation results are shown in Fig. 5, and we can observe that all the adsorption curves collapse into a single curve for $\sqrt{\tau} < 0.025$:

$$\frac{\psi_0(\tau)}{\psi_{eq}} \approx \frac{2.6}{\sqrt{\pi}}\sqrt{\tau}, \tag{43}$$

which is indeed independent of the choice of adsorption isotherm and ψ_b. However, the $\sqrt{\tau}$ behavior follows a different proportionality constant from the sharp interface model, which attributes to a finite thickness of the diffuse interface. It can also be found that the $\sqrt{\tau}$ behavior lasts shorter for $c/k_BT = 3$ and $\psi_b = 5 \times 10^{-3}$ compared to the other adsorption curves. This displays a stronger nonlinear adsorption process for large value of c/k_BT.

In the Ward and Tordai problem, the long-time adsorption behavior should be obtained numerically by solving Eq. (40) with a given adsorption isotherm. For the Langmuir adsorption, the long-time adsorption behavior can be approximated by [48]

$$\frac{\psi_0(\tau)}{\psi_{eq}} \approx 1 - \frac{\psi_c}{\psi_c\sqrt{\pi\tau} - \psi_b(1 - \sqrt{\pi\tau})}. \tag{44}$$

We note that the approximation of Eq. (44) corresponds to the long-time behavior in an infinite domain. Fig. 6 shows the simulation results of the whole adsorption process in the finite domain with $c = 0$, which are represented by the solid lines. It can be easily seen that the long-time adsorption behavior in

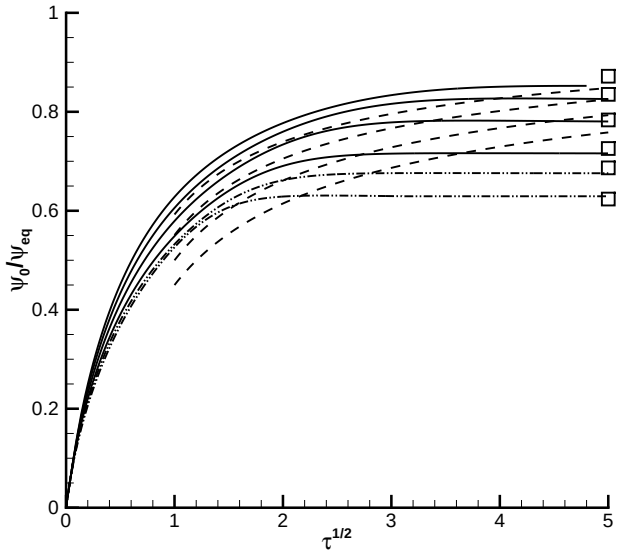

Figure 6: Evolution of surfactant concentration at the interface for the Langmuir adsorption with the initial bulk surfactant concentration $\psi_b = \{10^{-3}, 5 \times 10^{-3}, 10^{-2}, 1.5 \times 10^{-2}\}$ (the solid lines from bottom to top), as well as the Frumkin adsorption with $c = 2k_BT$ and $\psi_b = \{10^{-3}, 5 \times 10^{-3}\}$ (the dash-dot-dot lines from top to bottom). The dashed lines show the limiting behavior at $\tau \to \infty$ for the Langmuir adsorption, and the square symbols represent the analytical surfactant loadings in equilibrium.

a finite domain is different from an infinite domain. Compared with an infinite system, the finite system can equilibrate faster, which is more significant for a lower ψ_b. In a finite system, the initial ψ_b will change as the surfactants are adsorbed to the interface, leading to reduction of ψ_b, which will be more significant for a system with lower initial ψ_b. As the diffusion coefficient is ψ-dependent in our free energy model, the diffusion coefficient D_ψ cannot be accurately approximated by the initial bulk surfactant concentration ψ_b if it is small, whereas it is assumed a constant in obtaining Eq. (44). As the initial ψ_b increases, it can be expected that the adsorption behavior in a finite domain becomes closer to the approximation of Eq. (44), which is also reflected in Fig. 6. In addition, Fig. 6 also shows the whole adsorption processees in the finite domain with $c = 2k_BT$ and $\psi_b = \{10^{-3}, 5 \times 10^{-3}\}$, which are represented by dash-dot-dot lines. In contrast to the Langmuir adsorption, the Frumkin adsorption can equilibrate faster due to more surfactants absorbed to the interface. Finally, we compare the simulation results with the analytical solution of Eq. (27) when the finite system is in equilibrium. However, we cannot directly solve Eq. (27) to obtain the profile of surfactant concentration because the equilibrium bulk surfactant concentration ψ_b is unknown. For a closed system, the total mass of surfactant m_s should be conserved during the process of surfactant adsorption, i.e.

$$\int \psi \mathrm{d}x = m_s. \tag{45}$$

By satisfying the constraint of Eq. (45), we can use the two-step Newton's method to solve the nonlinear equation Eq. (27) to obtain the concentration profile. Details are given in Appendix C. Fig. 6 shows good agreement between simulation data and analytical solution for the equilibrium values of ψ_0/ψ_{eq}.

4.3. Surfactant effect on droplet dynamics

We have examined our model equilibrium behavior and surfactant adsorption dynamics. In this section, we apply the present phase-field model to investigate the droplet deformation, breakup and coalescence with the presence of surfactants in shear flows. All simulations are performed in a 2D rectangular domain with periodic boundary conditions on the left and right sides of the domain. The velocity boundary conditions [51] on the top and bottom sides of the domain are prescribed to introduce simple shear flow. The droplet is initially circular with the radius R, while the system

is initially at rest. The surfactant concentration starts with the analytical prediction of $\psi(\vec{x})$ for a given ψ_b. The characteristic length and velocity of simulation are chosen to be the droplet radius R and γR respectively, where γ is the shear rate. We introduce the following dimensionless numbers to classify the droplet dynamical behaviour:

$$\lambda = \frac{\eta_d}{\eta_m}, \quad Re = \frac{\rho\gamma R^2}{\eta_m}, \quad Ca = \frac{\gamma R \eta_m}{\sigma_0}, \tag{46}$$

where λ is the viscosity ratio of the droplet to the carrier fluid, which we set to be 1 here; Re is the Reynolds number; and Ca is the capillary number. When there are surfactants, interfacial tension will vary. In this case, we use the interfacial tension without surfactants to calculate Ca. In addition, we define the Peclet numbers Pe_ϕ and Pe_ψ, which are associated with the Cahn-Hilliard equations Eq. (14) and Eq. (15) respectively, as

$$Pe_\phi = \frac{\gamma R \xi}{|D_\phi|}, \quad Pe_\psi = \frac{\gamma R^2}{D_\psi}. \tag{47}$$

In the following simulations, we choose $\psi_c = 0.017$, $\xi/\delta_x = 2$, $Pe_\phi = 2$ and $Pe_\psi = 100$ so that the physical behavior of droplets in a typical oil/water/surfactant system can be reasonably reproduced.

4.3.1. Droplet deformation and breakup under shear

Here, we perform 2D simulation to examine the surfactant effect on droplet deformation and breakup under a shear flow. Initially, the droplet is circular with the radius $R = 32$, which is placed in the center of a 257×129 lattice flow domain. To study small deformation, we choose $Ca = 0.1$, $Re = 0.1$ and $\sigma_0 = 10^{-3}$. We investigate the effects of surfactant concentration and interaction coefficient c on droplet formation with two groups of parameters: $c = 0$ and $\psi_b = \{5 \times 10^{-3}, 10^{-2}, 1.5 \times 10^{-2}\}$; and $c/k_BT = \{0, 1, 2\}$ and $\psi_b = 10^{-2}$. For all the chosen parameters, it can be observed that the droplet deforms and eventually evolves to a stable elliptic shape, which is usually characterized by the Taylor deformation parameter, $Df = (L - B)/(L + B)$ with L and B being the major and minor axis of the ellipse. In Fig. 7, we have depicted the steady state shapes at $Ca = 0.1$, $Re = 0.1$ and $\sigma_0 = 10^{-3}$ for the clean droplet and the droplets with surfactants. For the droplet with surfactants, we have various ψ_b and c. For the Langmuir adsorption ($c = 0$), increasing surfactant concentration can lead to

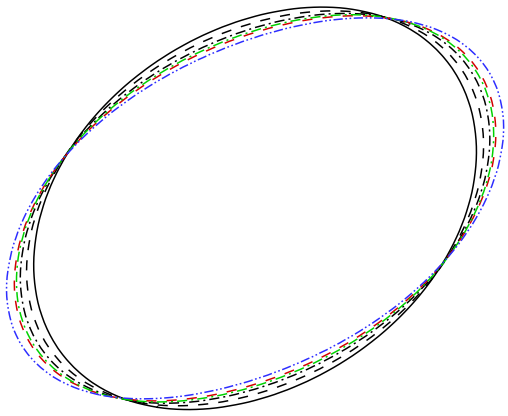

Figure 7: The stable shape of a droplet in the simple shear flow ($Ca = 0.1$, $Re = 0.1$ and $\sigma_0 = 10^{-3}$) with the presence of surfactants ($c = 0,\ \psi_b = 5 \times 10^{-3}$, the black dashed line; $c = 0,\ \psi_b = 10^{-2}$, the black dash-dot line; $c = 0,\ \psi_b = 1.5 \times 10^{-2}$, the red dashed line; $c = k_BT,\ \psi_b = 10^{-2}$, the green dash-dot line; $c = 2k_BT,\ \psi_b = 10^{-2}$, the blue dash-dot-dot line) and in the absence of surfactants (the black solid line).

a more prolate droplet. In addition, with the same surfactant concentration i.e. $\psi_b = 10^{-2}$, a large interaction coefficient c can also produce a highly enlongated droplet. The corresponding time evolution of Taylor deformation parameter is plotted in Fig. 8, which reveals the same observations.

During the droplet deformation, surfactant dilution due to the local interfacial stretching will counter the lowering of interfacial tension, and thus preventing the droplet further deformation. Meanwhile, the surfactants are gradually swept towards the droplet tips under the action of shear flow, resulting in the non-uniform distribution of the interfacial tension where the smallest interfacial tension occurs at the droplet tips. The Marangoni force will arise due to the gradient of interfacial tension, which resists the surfactants further migration. Consequently, the droplet may have a stable deformed shape. For the stable droplet, we also calculate the droplet inclination angle θ (the angle between the orientation of the major ellipse axis and the horizontal axis) using the method of moments [27]. The calculated inclination angles are: $\theta = 35.58$ degrees for the clean droplet, for the droplet with surfactants, θ is 32.76 degrees ($c = 0,\ \psi_b = 5 \times 10^{-3}$), 31.21 degrees ($c = 0,\ \psi_b = 10^{-2}$), 30.03 degrees ($c = 0,\ \psi_b = 1.5 \times 10^{-2}$), 30.33 degrees

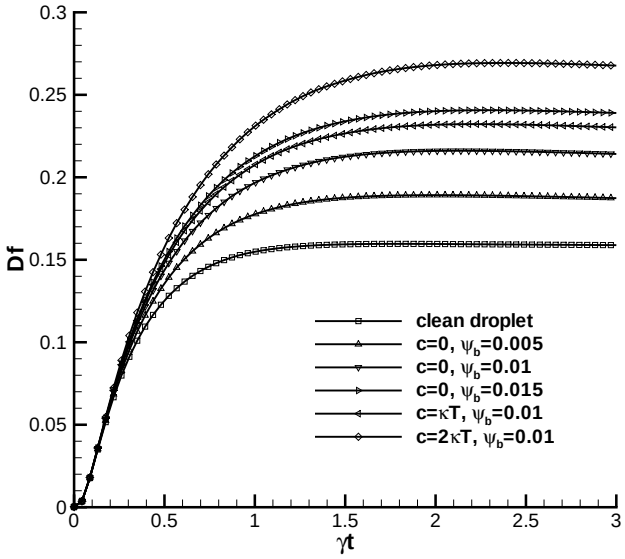

Figure 8: The time evolution of Taylor deformation parameter for a droplet in the shear flow with $Ca = 0.1$, $Re = 0.1$ and $\sigma_0 = 10^{-3}$.

($c = k_BT,\ \psi_b = 10^{-2}$), and 28.70 degrees ($c = 2k_BT,\ \psi_b = 10^{-2}$), respectively. The presence of surfactants acts to promote the droplet deformation and reduce the droplet inclination angle.

When we increase the capillary number and the Reynolds number, the droplet cannot evolve to a steady shape. Fig. 9 shows the time evolution plots of droplet deformation in the simple shear flow with $Ca = 0.5$, $Re = 1.0$ and $\sigma_0 = 10^{-3}$. The other parameters are kept to be the same as the above. As expected, the droplet deforms more significantly when ψ_b and c increase, which is consistent with the cases of small Ca and Re. If we continue to increase the capillary number and Reynolds number, a critical droplet state may appear, i.e. the droplet will breakup as the surfactant concentration exceeds a critical value. In order to capture the underlying physics of droplet breakup, we consider a 641×161 computational domain with a droplet of initial radius $R = 40$ lattices. The simulation starts with the clean droplet ($Ca = 0.6$, $Re = 2.4$ and $\sigma_0 = 10^{-3}$). As the surfactant concentration increases, Fig. 10 shows that the droplet breakup begins at some critical value for both $c = 0$ and $c = 2k_BT$. When the droplet breakup occurs, the

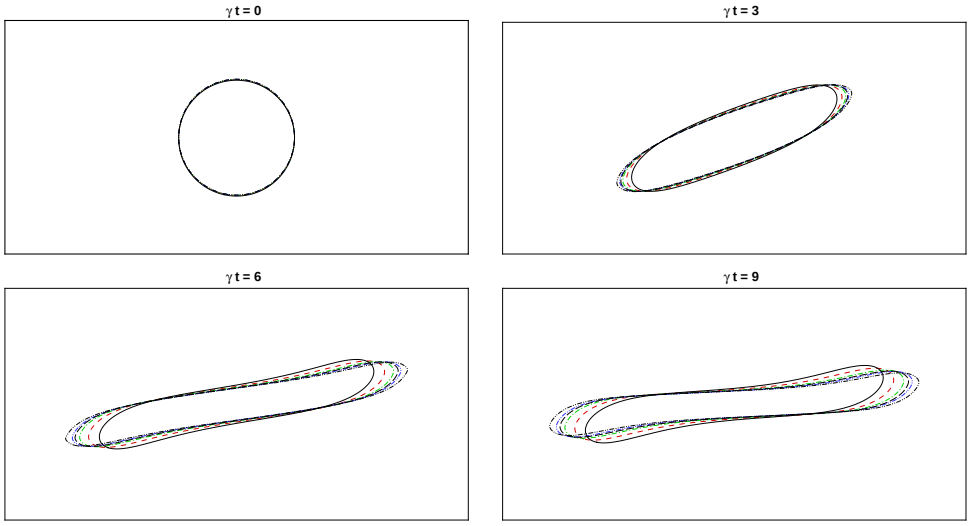

Figure 9: The time evolution of a droplet in the shear flow ($Ca = 0.5$, $Re = 1.0$ and $\sigma_0 = 10^{-3}$) with the presence of surfactants ($c = 0,\ \psi_b = 5 \times 10^{-3}$, the red dashed line; $c = 0,\ \psi_b = 10^{-2}$, the green dash-dot line; $c = 0,\ \psi_b = 1.5 \times 10^{-2}$, the blue dash-dot-dot line; $c = k_BT,\ \psi_b = 10^{-2}$, the black long-dash line; $c = 2k_BT,\ \psi_b = 10^{-2}$, the black dash-dot-dot line) and in the absence of surfactants (the black solid line).

increasing of ψ_b or c can accelerate the droplet breakup process, and smaller daughter droplets will be generated. In addition, we notice that the droplet will shrink again once the maximal deformation is not enough to "pinch-off" the droplet.

4.3.2. Collision of two equal-sized droplets

We consider the effect of surfactant dynamics on droplet-droplet interactions in the simple shear flow with $Ca = 0.1$, $Re = 0.4$ and $\sigma_0 = 10^{-3}$. We consider two initially circular droplets with the radius of 40 lattices and located at (101, 141) and (261, 101). The 2D computational domain is 361×241. In Fig. 11, the droplet evolution is shown at the times (γt) of 0, 2.5, 5.0, 5.5, 7.5 and 8.0. We find that the droplet coalescence due to collision is dramatically hindered by the presence of surfactant molecules, which has also been experimentally observed [8, 52, 53, 54]. The surfactants have little effect on the droplet behavior, until the two droplets move close to each other. When the two droplets are in close contact, the surfactant concentration and the adsorption isotherm have significant influence on droplet coalescence. The increase of ψ_b or c prevents the droplets from merging.

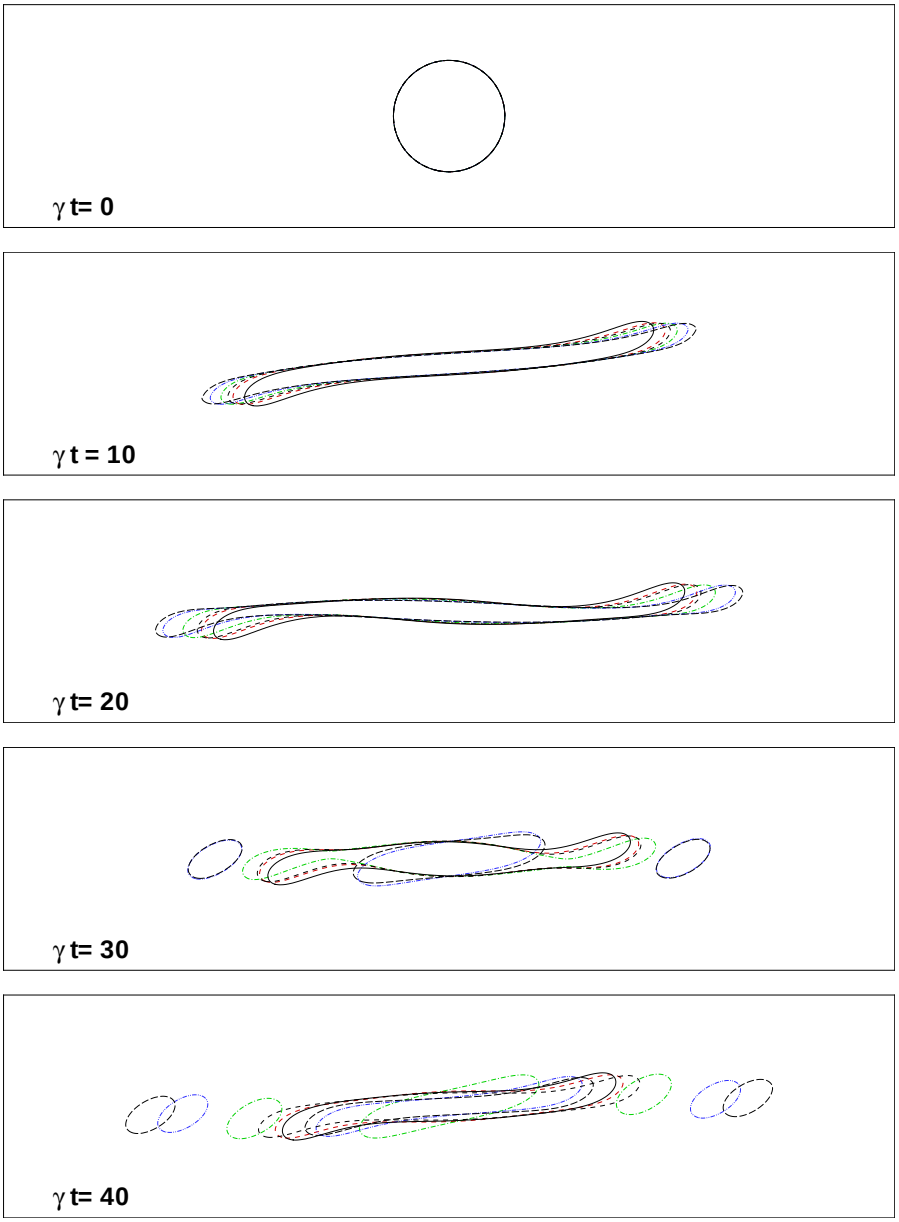

Figure 10: Evolution of droplet breakup in the shear flow ($Ca = 0.6$, $Re = 2.4$ and $\sigma_0 = 10^{-3}$) with the presence of surfactants ($c = 0$, $\psi_b = 5 \times 10^{-3}$, the red dashed line; $c = 0$, $\psi_b = 10^{-2}$, the green dash-dot line; $c = 0$, $\psi_b = 1.5 \times 10^{-2}$, the blue dash-dot-dot line; $c = 2k_BT$, $\psi_b = 5 \times 10^{-3}$, the black dashed line; $c = 2k_BT$, $\psi_b = 10^{-2}$, the black long-dash line.) and in the absence of surfactants (the black solid line).

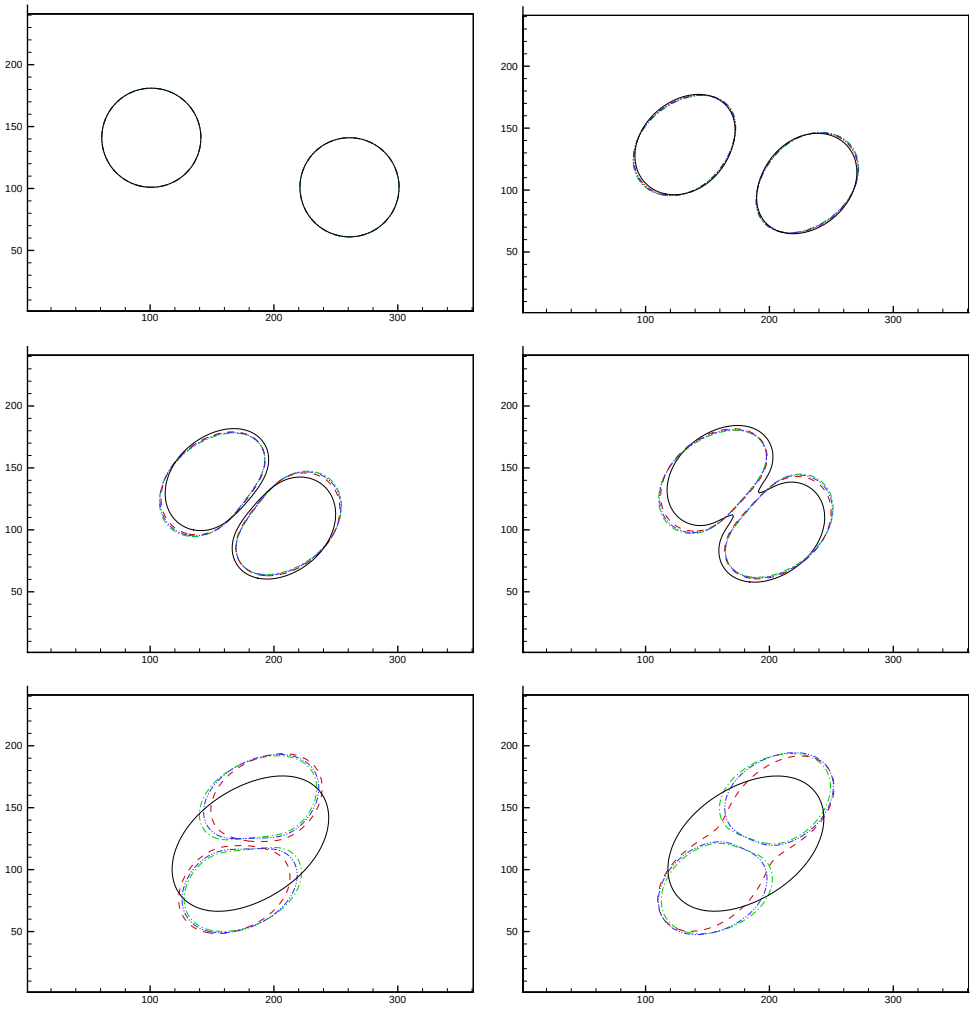

Figure 11: The glancing collision of two droplets in the shear flow ($Ca = 0.1$, $Re = 0.4$ and $\sigma_0 = 10^{-3}$) with the presence of surfactants ($c = 0$, $\psi_b = 5 \times 10^{-3}$, the red dashed line; $c = 0$, $\psi_b = 10^{-2}$, the green dash-dot line; $c = 2k_BT$, $\psi_b = 5 \times 10^{-3}$, the blue dash-dot-dot line) and in the absence of surfactants (the black solid line).

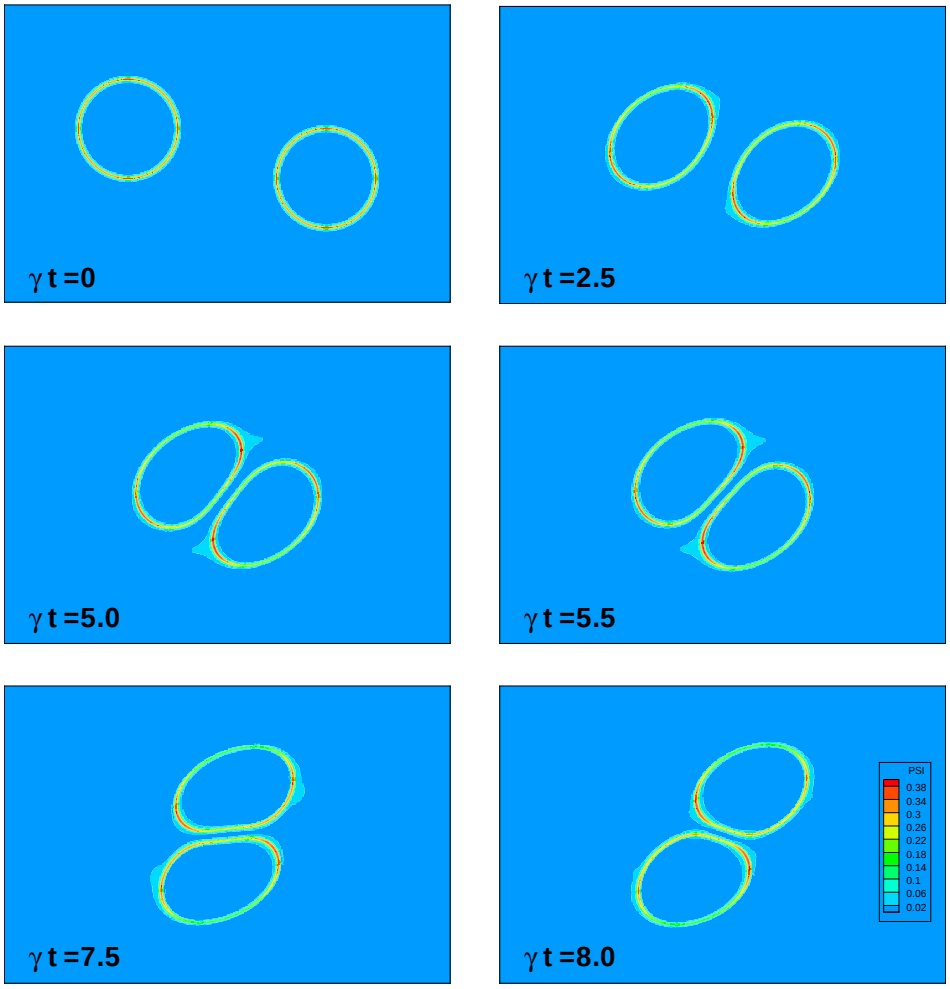

Figure 12: Evolution of surfactant concentration of two colliding droplets in the simple shear flow ($Ca = 0.1$, $Re = 0.4$, $\sigma_0 = 10^{-3}$, $c = 0$, and $\psi_b = 10^{-2}$).

Fig. 12 shows the contour plot of surfactant concentration of two colliding droplets in the simple shear flow ($\psi_b = 10^{-2}$ and $c = 0$). At the beginning, the surfactant molecules are convected towards the droplet tips. As the two droplets approach each other, the increased pressure in the gap between the two droplets pushes surfactants away from the near-contact region. We can clearly see that the surfactant concentrations are unevenly distributed along the interfaces, thus generating the Marangoni stress that affects the droplet-droplet interaction. In addition, the reduction of interfacial tension due to the presence of surfactants can enhance droplet deformation, and thus affect droplet-droplet interaction as well. The dimple forming in the near-contact region, which has been observed during the collision of two droplets using the sharp interface model with insoluble surfactant [12, 13], is not clear in our simulations. It is because the dimple is produced by the a high repulsive lubrication pressure at $h \ll R$ (h is the gap between two droplets), whereas the diffuse interface model underpredicts the lubrication pressure when $h/\xi < 1.5$ [55].

As we know, the increase of the effective capillary number (Ca_e) due to the presence of surfactants can inhibit the droplet coalescence. However, what is the role of Marangoni stress during the droplet coalescence? To answer this question, we have simulated two cases where the effective capillary number is the same, i.e. $Ca_e = 0.1$, for the droplets with surfactants ($c = 0, \psi_b = 10^{-2}$) and the clean droplet. The other parameters are kept the same as the above. The effective capillary number is defined by

$$Ca_e = \frac{\gamma R \eta_m}{\sigma_e}, \tag{48}$$

where σ_e is the initial equilibrium interfacial tension, which is the same to σ_0 for the clean droplet and smaller than σ_0 for the droplets with surfactants. To ensure the two cases having the same effective interfacial tension, we need to calculate the required σ_0 for the droplets with surfactants as

$$\sigma_0 = \frac{\sigma_e}{1 - \frac{0.375\alpha}{\xi \ln \psi_c}(1 + \frac{1}{Ex})[\ln(1 - \psi_0) + \frac{1}{2}\tilde{c}\psi_0^2]}. \tag{49}$$

Therefore, σ_0 is different for the two cases.

In the present simulation, α is 2.0 for $Ex = 0.25$. Fig. 13 shows the evolution of droplet collision with $Ca_e = 0.1$, $Re = 0.4$ and $\sigma_e = 10^{-3}$ (in the presence of surfactants, $c = 0$ and $\psi_b = 10^{-2}$). Although the two cases have

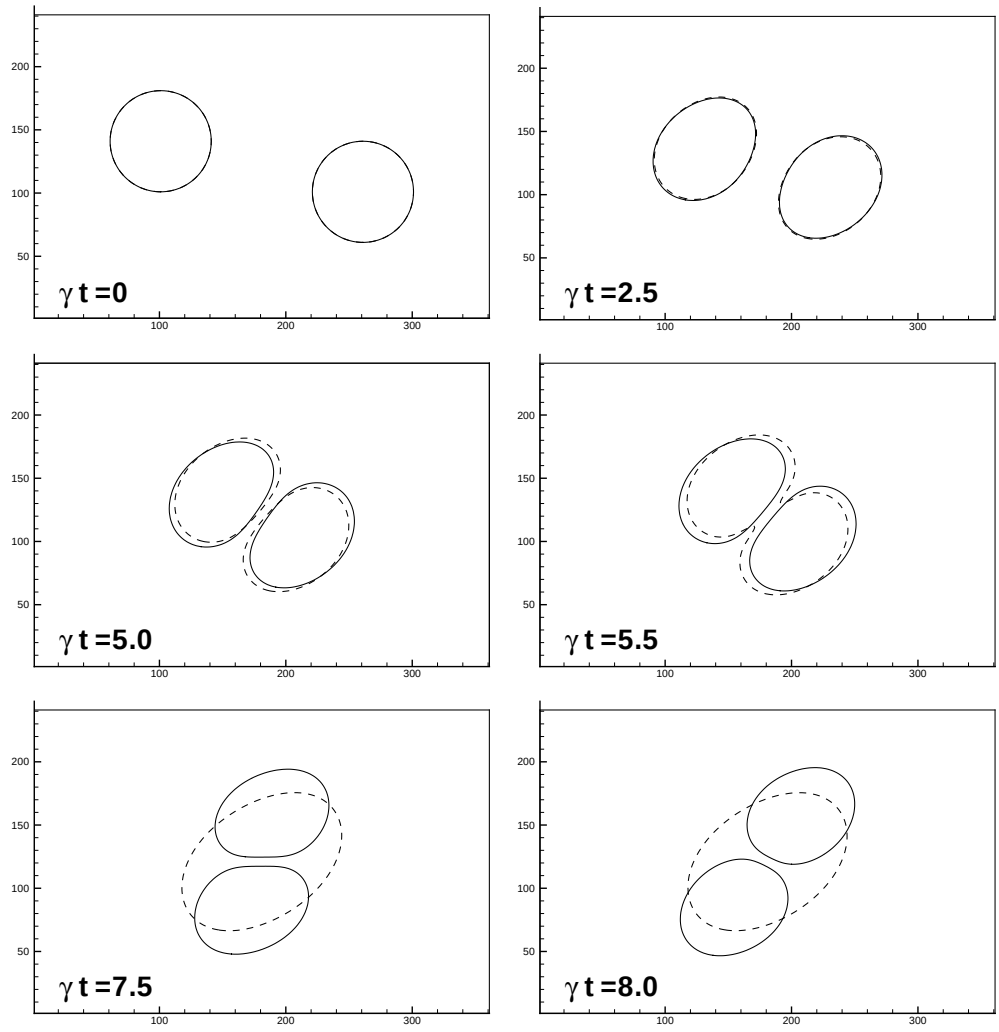

Figure 13: The glancing collision of two droplets in the shear flow ($Ca_e = 0.1$, $Re = 0.4$ and $\sigma_e = 10^{-3}$) with the presence of surfactants ($c = 0,\ \psi_b = 10^{-2}$, the solid line) and in the absence of surfactants (the dashed line).

the same effective capillary number, it can be found that the Marangoni stress induced by non-uniform interfacial tension acts as an additional repulsive force to prevent droplet coalescence.

To show the effect of Marangoni stress on the flowfield, Fig. 14(a) gives the comparison of the velocity vectors in the vicinity of the gap at the drainage time $\gamma t = 4.0$ with surfactants ($c = 0$ and $\psi_b = 10^{-2}$, the red arrows) and without surfactants (the blue arrows). It can be clearly seen that the gap between the two droplets without surfactants is more narrow, which indicates that the presence of surfactants does slow down the film drainage process and thus increases the required drainage time prior to coalescence. It has been demonstrated that the surfactants can immobilize the bubble interface due to the effect of Marangoni stress during the motion of buoyancy-driven bubbles in a circular tube [14]. The Marangoni stress can also lead to reduction of the interface mobility during the droplet-droplet interaction, though the reduction is not as significant as that in the bubble deformation, where the viscosity ratio of bubble to carrier fluid is small. The Peclet number will increase as the mobility decreases, which can lead to droplet collision-separation [56]. Fig. 14(b) shows the flowfield at $\gamma t = 6.5$ ($c = 0$ and $\psi_b = 10^{-2}$), where the streamlines are self-closed circle-like with the two droplets rotating like rigid bodies, which was also observed by Yu and Zhou [56].

As found from the above, the presence of surfactants can increase the droplet deformation and reduce the droplet inclination angle. We also know that the presence of surfactants leads to the increase of Ca_e, which can increase the droplet deformation and reduce the droplet inclination angle. To understand the mechanism of droplet deformation when the surfactants are present. We re-examine the droplet deformation with three groups of different parameters: 1) clean droplet with $Ca = Ca_e = 0.1$, $Re = 0.1$ and $\sigma_0 = \sigma_e = 10^{-3}$; 2) contaminated droplet with $Ca = 0.1$, $Re = 0.1$, $\sigma_0 = 10^{-3}$, $\psi_b = 10^{-2}$ and $c = 0$, so that $Ca_e = 0.127$ and $\sigma_e = 7.87 \times 10^{-4}$; and 3) clean droplet with $Ca = Ca_e = 0.127$, $Re = 0.1$ and $\sigma_0 = \sigma_e = 7.87 \times 10^{-4}$. The group 3 has the same effective capillary number as the group 2, which is designed to single out the effect of the increase of Ca_e on droplet deformation when the surfactants are added. Fig. 15 gives the evolutions of Taylor deformation parameter for the above three groups of data. The total amount of deformation Δ has two parts: Δ_1, due to the Marangoni stresses induced by redistribution of the surfactants, and Δ_2, stemming from the increase of Ca_e due to the surfactant adsorption. For the present case, it is clear that the effect of Marangoni stresses is significant. We expect that the

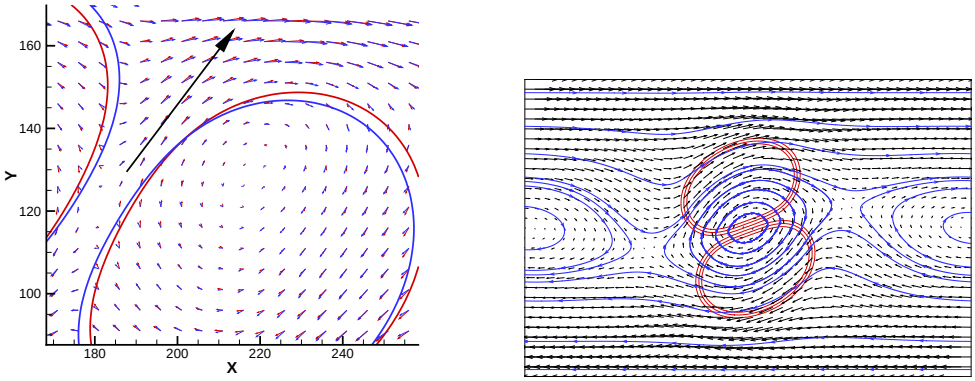

(a) (b)

Figure 14: (a) Velocity vectors are shown at every fifth grid point in the vicinity of the gap at $\gamma t = 4.0$ ($Ca_e = 0.1$, $Re = 0.4$ and $\sigma_e = 10^{-3}$). The red line is the droplet interface with the surfactants while the blue line is the interface of the clean droplet. (b) The flowfield is shown at every eighth grid point ($\gamma t = 7.0$) for droplets collision-separation in the presence of surfactants ($c = 0$ and $\psi_b = 10^{-2}$). The red solid lines are ϕ contours of 0 and ± 0.8, the blue lines are the streamlines.

Marangoni stresses are smaller for the soluble surfactants than the insoluble ones due to the bulk diffusion, which can redistribute the surfactants through desorption from the droplet tips and adsorption in the middle regions of the droplet. The steady inclination angle is obtained with $\theta = 33.23$ degrees for the group 3 in contrast to $\theta = 35.58$ degrees for the group 1 and $\theta = 31.21$ degrees for the group 2. Therefore, when the surfactants are presented, the Marangoni stresses and the increase of Ca_e are responsible for the increase of the droplet deformation and the reduction of the droplet inclination angle.

It has been argued that Pe_ϕ can affect the interfacial dynamics to some extent in the phase field model [27, 56]. It is different from the other Peclet number Pe_ψ, though both are associated with the Cahn-Hilliard equations in the same form. Pe_ψ is a physical dimensionless parameter relating convection to diffusion of surfactants in the bulk phases, whereas Pe_ϕ is a purely numerical parameter, indicating the interface diffusivity, which is unique to phase field model. The moderate interface diffusion is numerically desirable to avoid spurious velocities and numerical instability at the interface. While straining flows, which can thicken or thin the interface, must be balanced by diffusion, large diffusion will excessively damp the flow. Here, we investigate

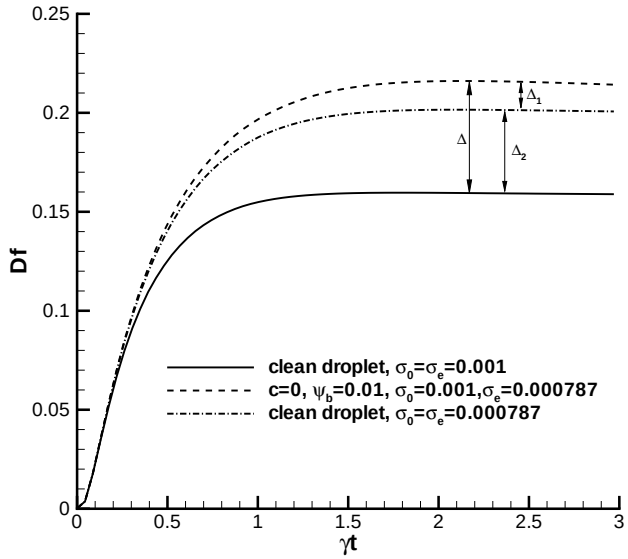

Figure 15: The time evolution of Taylor deformation parameter for a droplet in the shear flow with $Ca = 0.1$, $Re = 0.1$ and $\sigma_e = 10^{-3}$.

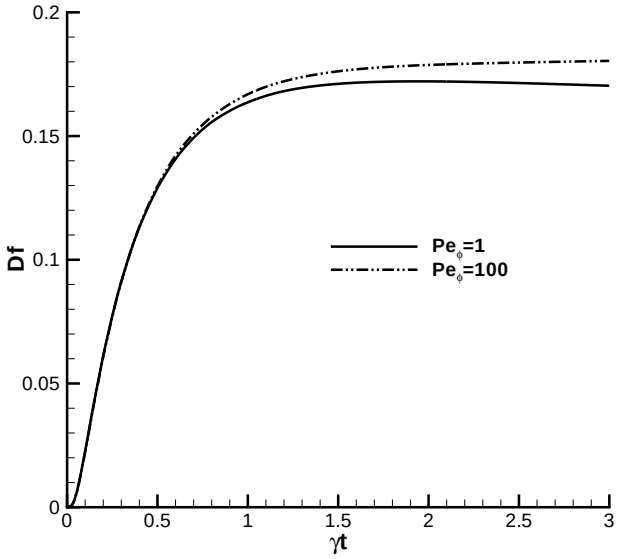

Figure 16: The influence of Pe_ϕ on the evolution of Taylor deformation parameter for a droplet in the shear flow with $Ca_e = 0.1$, $Re = 0.1$, $c = 0$, $\psi_b = 0.01$ and $Pe_\psi = 100$.

the influence of Pe_ϕ on the droplet deformation for $Ca_e = 0.1$, $Re = 0.1$, $c = 0$, $\psi_b = 0.01$ and $Pe_\psi = 100$. The value of Pe_ϕ is obtained by varying M_ϕ (Γ_ϕ), and all the other parameters are kept to be the same. Fig. 16 shows that the time evolution of Taylor deformation parameter Df for $Pe_\phi = 1$ and 100. It can been clearly seen that Pe_ϕ can increase the droplet deformation at a constant Ca_e. Also, the droplet is continuously deformed and no steady state is observed for $Pe_\phi = 100$. Note, the analogous Weber number, defined as $We_\xi = \frac{\sigma_0/\xi}{\rho c_s^2}$, in the above simulations ranges from 1.5×10^{-3} to 3×10^{-2}. Finally, the coupling term $\frac{w}{2}\psi\phi^2$ in the free energy functional is essential for numerical stability. Since $Ex = \frac{d}{w\xi^2}$, Ex can indirectly influence stability. We observed numerical stability problem at large Ex which corresponds to small w. In our simulations, we found that $Ex \leq 0.5$ is a good choice for $\psi_c = 0.017$ and $10^{-3} \leq \psi_b \leq 1.5 \times 10^{-2}$.

5. Conclusions

We have proposed a generalized free energy functional to enable the phase-field model to capture surfactant dynamics in a multiphase system with the bulk surfactant concentration below CMC. In comparison with the other multiphase/surfactant models, the present model can describe evolution of the interface and the surfactant concentration automatically. In equilibrium, this model can lead to the commonly-used surfactant adsorption isotherms, i.e. the Langmuir and Frumkin isotherms. In addition, our model can deal with different solubility of surfactants in the bulk phases. The lowering of interfacial tension caused by the surfactant concentration at the interface, is theoretically and numerically analyzed.

For the Ward and Tordai problem, the interface surfactant loading ψ_0/ψ_{eq} follows $\sqrt{\tau}$ behavior at short-time. At long-time, we find that the surfactant adsorption behavior in a finite system is significantly different from an infinite system as the finite system can equilibrate faster. The surfactant concentration ψ_b and the interaction coefficient c have been found to have big impact on the droplet formation, breakup and collision in a simple shear flow. The increase of ψ_b and c can promote the droplet deformation, decrease the droplet inclination angle, and acceralate the droplet breakup. Smaller daughter droplets are expected to emit for large ψ_b or c. The droplets will less likely to merge when the surfactants are introduced, and the increase of ψ_b and c makes the droplet coalescence more difficult. The reasons are that the effective capillary number is increased due to the reduction of interfacial tension, and the time required for film drainage to the point of film rupture is increased due to the Marangoni effect.

Acknowledgments

The authors would like to thank R.G.M. van der Sman for the valuable discussions.

Appendix A. The equilibrium properties

The free energy functional is chosen as Eq. (5). The excess free energy per unit interface area can be defined by

$$W(\phi,\psi) = f(\phi,\psi) - f(\phi_b,\psi_b) - \frac{\partial f(\phi_b,\psi_b)}{\partial \phi_b}(\phi-\phi_b) - \frac{\partial f(\phi_b,\psi_b)}{\partial \psi_b}(\psi-\psi_b), \tag{A.1}$$

which satisfies the Euler-Lagrange minimization equations:

$$\frac{\partial W}{\partial \phi} - \frac{\mathrm{d}}{\mathrm{d}x}\left(\frac{\partial W}{\partial \nabla \phi}\right) = 0, \tag{A.2}$$

$$\frac{\partial W}{\partial \psi} - \frac{\mathrm{d}}{\mathrm{d}x}\left(\frac{\partial W}{\partial \nabla \psi}\right) = 0. \tag{A.3}$$

Defining $\eta(x) = \phi(x)/\phi_b$, and from Eqs. (A.1), (A.2) and (A.3), we obtain:

$$\begin{aligned} W &= k_B T\left[\psi \ln\left(\frac{\psi}{\psi_b}\right) + (1-\psi)\ln\left(\frac{1-\psi}{1-\psi_b}\right)\right] - \frac{c}{2}(\psi-\psi_b)^2 \\ &\quad + \frac{w}{2}\phi_b^2(\psi-\psi_b)(\eta^2-1) + \frac{b}{4}\phi_b^4(\eta^2-1)^2 + \frac{1}{2}(\kappa - d\psi)\,\phi_b^2\eta_x^2, \end{aligned} \tag{A.4}$$

$$b\phi_b^3(\eta^3-\eta) + w\phi_b\eta(\psi-\psi_b) = (\kappa - d\psi)\phi_b\eta_{xx} - d\phi_b\eta_x\psi_x, \tag{A.5}$$

$$k_B T\left[\ln\left(\frac{\psi}{\psi_b}\right) - \ln\left(\frac{1-\psi}{1-\psi_b}\right)\right] - c(\psi-\psi_b) + \frac{w}{2}\phi_b^2(\eta^2-1) - \frac{d}{2}\phi_b^2\eta_x^2 = 0. \tag{A.6}$$

When the surfactant excess is moderate at the interface, we can rewrite Eq. (A.6) using a linear approximation for the logarithmic part as:

$$\chi(\psi-\psi_b) + \frac{w}{2}\phi_b^2(\eta^2-1) - \frac{d}{2}\phi_b^2\eta_x^2 \approx 0, \tag{A.7}$$

where $\chi = k_B T\left(\frac{1}{\psi_b} + \frac{1}{1-\psi_b}\right) - c$.

From Eq. (A.7), we obtain

$$\psi - \psi_b = \frac{\phi_b^2}{2\chi}[w(1-\eta^2) + d\eta_x^2], \tag{A.8}$$

$$\psi_x = \frac{1}{\chi}\phi_b^2\eta_x(d\eta_{xx} - w\eta). \tag{A.9}$$

Substituting Eqs. (A.8) and (A.9) into Eq. (A.5), we have

$$\begin{aligned} &b\phi_b^3(\eta^3-\eta) + \frac{w\phi_b^3}{2\chi}\eta[w(1-\eta^2) + d\eta_x^2] = -\frac{d\phi_b^3}{\chi}\eta_x^2(d\eta_{xx} - w\eta) \\ &+ \left\{\kappa - d\psi_b - \frac{\phi_b^2 d}{2\chi}[w(1-\eta^2) + d\eta_x^2]\right\}\phi_b\eta_{xx}. \end{aligned} \tag{A.10}$$

The interfacial profile $\eta(x)$ can be obtained by the solution of Eq. (A.10). Unfortunately, Eq. (A.10) cannot be analytically solved. To obtain an expression for the interfacial tension σ, we omit all the high-order terms in Eq. (A.10), so that the equation is simplified as:

$$b\phi_b^3(\eta^3-\eta)+\frac{w\phi_b^3}{2\chi}w\eta(1-\eta^2)=\left(\kappa-d\psi_b-\frac{1}{2\chi}dw\phi_b^2\right)\phi_b\eta_{xx}. \tag{A.11}$$

Therefore, we can obtain

$$\eta(x)=\tanh(x/\xi), \tag{A.12}$$

where

$$\xi^2=\frac{2\left[\kappa-d\left(\psi_b+\frac{\phi_b^2 w}{2\chi}\right)\right]}{\phi_b^2\left(b-\frac{w^2}{2\chi}\right)}. \tag{A.13}$$

In our free energy model given by Eq. (5), χ can be approximated by $\chi\approx k_BT/\psi_b$ due to c is up to $\mathcal{O}(k_BT)$ and $\psi_b\ll 1$. Therefore, Eq. (A.13) can be approximated by:

$$\xi^2=\frac{2\kappa}{b\phi_b^2}, \tag{A.14}$$

which accords with our assumption that the solvent composition profile is independent of the surfactant loading in equilibrium. When $\chi=c$, the free energy model proposed by Theissen and Gompper [31] can be recovered with the parameter of interface thickness defined by Eq. (4). By integrating the excess free energy per unit interface area i.e. Eq. (A.4) in the whole domain, we can obtain the interfacial tension i.e. Eq. (3) for $\chi=c$.

Appendix B. Equilibrium distributions

Following the constraints of Eqs.(31) and (35), the equilibrium distributions, which are assumed to be a power series in terms of the local velocity, can be written as:

$$\begin{aligned}
f_i^{eq} &= F_i+w_i\rho\left[\frac{\vec{e}_i\cdot\vec{u}}{c_s^2}+\frac{(\vec{e}_i\cdot\vec{u})^2}{2c_s^4}-\frac{\vec{u}\cdot\vec{u}}{2c_s^2}\right],\\
g_i^{eq} &= G_i+w_i\phi\left[\frac{\vec{e}_i\cdot\vec{u}}{c_s^2}+\frac{(\vec{e}_i\cdot\vec{u})^2}{2c_s^4}-\frac{\vec{u}\cdot\vec{u}}{2c_s^2}\right],\\
h_i^{eq} &= H_i+w_i\psi\left[\frac{\vec{e}_i\cdot\vec{u}}{c_s^2}+\frac{(\vec{e}_i\cdot\vec{u})^2}{2c_s^4}-\frac{\vec{u}\cdot\vec{u}}{2c_s^2}\right].
\end{aligned} \tag{B.1}$$

for $i = 1, ..., 8$, where

$$F_i = \begin{cases} \vec{e}_i^{\mathrm{T}} \mathbf{P} \vec{e}_i / 2c^4 - (P_{xx} + P_{yy})/12c^2 & i = 1 - 4, \\ \vec{e}_i^{\mathrm{T}} \mathbf{P} \vec{e}_i / 8c^4 - (P_{xx} + P_{yy})/6c^2 & i = 5 - 8. \end{cases} \tag{B.2}$$

and

$$G_i = \frac{1}{c_s^2} w_i \Gamma_\phi \mu_\phi, \quad H_i = \frac{1}{c_s^2} w_i \Gamma_\psi \mu_\psi. \tag{B.3}$$

The stationary values i.e. $i = 0$ are chosen to conserve the mass of each species,

$$f_0^{eq} = \rho - \sum_{i=1}^{8} f_i^{eq}, \quad g_0^{eq} = \phi - \sum_{i=1}^{8} g_i^{eq}, \quad h_0^{eq} = \psi - \sum_{i=1}^{8} h_i^{eq}. \tag{B.4}$$

Appendix C. Newton method for solution of equilibrium surfactant concentration in a closed system

We use a two-step Newton's method to solve the equilibrium surfactant concentration in a closed system with a given total surfactant concentration m_s. In equilibrium, the surfactant concentration follows the Eq. (27), which can be rewritten as

$$\psi(x) = \frac{1}{1 + y \mathrm{e}^{-\tilde{c}\psi(x)} \vartheta(x)}, \tag{C.1}$$

where $\vartheta(x) = \exp\left\{ \frac{1}{k_B T} \left[\frac{w}{2} \phi^2 - \frac{\kappa}{2} (\partial_x \phi)^2 \right] \right\}$, $y = \mathrm{e}^{-\frac{1}{k_B T} \mu_\psi}$, and $\tilde{c} = \frac{c}{k_B T}$. Meanwhile, the surfactant concentration must satisfy the constraint of Eq. (45), which can be expressed in a discrete form:

$$\sum_i \psi(x_i) \delta_x = m_s \tag{C.2}$$

We introduce the notations: $\psi_i = \psi(x_i)$, $\vartheta_i = \vartheta(x_i)$, and directly substitute Eq. (C.1) into Eq. (C.2). Therefore, Eqs. (C.1) and (C.2) become

$$\psi_i = \frac{1}{1 + y \mathrm{e}^{-\tilde{c}\psi_i} \vartheta_i}, \tag{C.3}$$

$$\sum_i \frac{1}{1 + y \mathrm{e}^{-\tilde{c}\psi_i} \vartheta_i} \delta_x = m_s. \tag{C.4}$$

In the above equations, ψ_i and y are unknowns. We can use the following algorithm to obtain the unknowns.

1. Set $k = 0$, and give y an initial guess y^0.
2. Set $y = y^k$, and use the Newton-Raphson method to iteratively solve Eq. (C.3) until a converged solution ψ_i^k is obtained at all the lattice points.
3. Set $\psi_i = \psi_i^k$ for all the lattice points, and then use the Newton-Raphson method to iteratively solve Eq. (C.4) until a converged solution y^{k+1} is obtained. Update $k = k + 1$.
4. Repeat the solution steps (2) and (3) until the solutions satisfy the given conditions.

References

[1] J. Sjöblom, Emulsions and Emulsion Stability, Taylor & Francis, 2006.

[2] H. Stone, A. Stroock, A. Ajdari, Engineering flows in small devices microfluidics toward a lab-on-a-chip, Annu. Rev. Fluid Mech. 36 (2004) 381–411.

[3] J.-C. Baret, F. Kleinschmidt, A. El Harrak, A. D. Griffiths, Kinetic aspects of emulsion stabilization by surfactants: A microfluidic analysis, Langmuir 25 (11) (2009) 6088–6093.

[4] P. Tabeling, Introduction to microfluidics, Oxford: Oxford University Press, 2005.

[5] S. van der Graaf, M. L. J. Steegmans, R. G. M. van der Sman, C. G. P. H. Schroën, R. M. Boom, Droplet formation in a T-shaped microchannel junction: A model system for membrane emulsification, Colloids Surf. A 266 (2005) 106–116.

[6] M. L. J. Steegmans, A. Warmerdam, K. G. P. H. Schroën and R. M. Boom, Dynamic interfacial tension measurements with microfluidic Y-junctions, Langmuir 25 (17) (2009) 9751–9758.

[7] H. A. Stone, L. G. Leal, The effects of surfactants on drop deformation and breakup, J. Fluid Mech. 220 (1990) 161–186.

[8] U. Sundararaj, C. Macosko, Drop breakup and coalescence in polymer blends - the effects of concentration and compatibilization, Macromolecules 28 (1995) 2647–2657.

[9] P. V. Puyvelde, S. Velankar, J. Mewis, P. Moldenaers, K. U. Leuven, Effect of marangoni stresses on the deformation and coalescence in compatibilized immiscible polymer blends, Polym. Eng. Sci. 42 (10) (2002) 1956–1964.

[10] L. G. Leal, Flow induced coalescence of drops in a viscous fluid, Phys. Fluids 16 (6) (2004) 1833–1851.

[11] S. L. Anna, H. C. Mayer, Microscale tipstreaming in a microfluidic flow focusing device, Phys. Fluids 18 (12) (2006) 121512.

[12] J.-J. Xu, Z. Li, J. Lowengrub, H. Zhao, A level-set method for interfacial flows with surfactant, J. Comput. Phys. 212 (2) (2006) 590 – 616.

[13] B. Dai, L. G. Leal, The mechanism of surfactant effects on drop coalescence, Phys. Fluids 20 (4) (2008) 040802.

[14] S. Tasoglu, U. Demirci, M. Muradoglu, The effect of soluble surfactant on the transient motion of a buoyancy-driven bubble, Phys. Fluids 20 (4) (2008) 040805.

[15] J. Eastoe, J. S. Dalton, Dynamic surface tension and adsorption mechanisms of surfactants at the air-water interface, Adv. Colloid Interface Sci. 85 (2-3) (2000) 103 – 144.

[16] H. D. Ceniceros, The effects of surfactants on the formation and evolution of capillary waves, Phys. Fluids 15 (1) (2003) 245–256.

[17] A. J. James, J. Lowengrub, A surfactant-conserving volume-of-fluid method for interfacial flows with insoluble surfactant, J. Comput. Phys. 201 (2) (2004) 685 – 722.

[18] M. A. Drumright-Clarke, Y. Renardy, The effect of insoluble surfactant at dilute concentration on drop breakup under shear with inertia, Phys. Fluids 16 (1) (2004) 14–21.

[19] J. Lee, C. Pozrikidis, Effect of surfactants on the deformation of drops and bubbles in Navier-Stokes flow, Comput. Fluids 35 (1) (2006) 43 – 60.

[20] M.-C. Lai, Y.-H. Tseng, H. Huang, An immersed boundary method for interfacial flows with insoluble surfactant, J. Comput. Phys. 227 (15) (2008) 7279 – 7293.

[21] M. Muradoglu, G. Tryggvason, A front-tracking method for computation of interfacial flows with soluble surfactants, J. Comput. Phys. 227 (4) (2008) 2238–2262.

[22] H. Diamant, D. Andelman, Kinetics of surfactant adsorption at fluid-fluid interfaces, J. Phys. Chem. 100 (1996) 13732.

[23] K. N. Premnath, J. Abraham, Simulations of binary drop collisions with a multiple-relaxation-time lattice-Boltzmann model, Phys. Fluids 17 (12) (2005) 122105.

[24] S. van der Graaf, T. Nisisako, C. G. P. H. Schroën, R. G. M. van der Sman, R. M. Boom, Lattice Boltzmann simulations of droplet formation in a T-shaped microchannel, Langmuir 22 (9) (2006) 4144–4152.

[25] H. Zheng, C. Shu, Y. Chew, A lattice Boltzmann model for multiphase flows with large density ratio, J. Comput. Phys. 218 (1) (2006) 353–371.

[26] T. Lee, P. F. Fischer, Eliminating parasitic currents in the lattice Boltzmann equation method for nonideal gases, Phys. Rev. E 74 (4) (2006) 046709.

[27] R. van der Sman, S. van der Graaf, Emulsion droplet deformation and breakup with lattice Boltzmann model, Comput. Phys. Commun. 178 (7) (2008) 492–504.

[28] J. Huang, C. Shu, Y. Chew, Numerical investigation of transporting droplets by spatiotemporally controlling substrate wettability, J. Coll. Interf. Sci. 328 (1) (2008) 124–133.

[29] H. Liu, Y. Zhang, Droplet formation in a T-shaped microfluidic junction, J. Appl. Phys. 106 (6) (2009) 034906.

[30] P. M. Chaikin, T. C. Lubensky, Principles of Condensed Matter Physics, Cambridge: Cambridge University Press, 2000.

[31] O. Theissen, G. Gompper, Lattice-Boltzmann study of spontaneous emulsification, Eur. Phys. J. B 11 (1) (1999) 91–100.

[32] R. van der Sman, S. van der Graaf, Diffuse interface model of surfactant adsorption onto flat and droplet interfaces, Rheol. Acta 46 (1) (2006) 3–11.

[33] K. Furtado, C. M. Pooley, J. M. Yeomans, Lattice Boltzmann study of convective drop motion driven by nonlinear chemical kinetics, Phys. Rev. E 78 (2008) 046308.

[34] M. R. Swift, E. Orlandini, W. R. Osborn, J. M. Yeomans, Lattice Boltzmann simulations of liquid-gas and binary fluid systems, Phys. Rev. E 54 (5) (1996) 5041–5052.

[35] M. Laradji, H. Guo, M. Grant, M. J. Zuckermann, The effect of surfactants on the dynamics of phase separation, J. Phys. Condens. Matter 4 (1992) 6715–6728.

[36] A. Halperin, P. Pincus, Polymers at a liquid-liquid interface, Macromolecules 19 (1) (1986) 79–84.

[37] V. M. Kendon, M. E. Cates, I. Pagonabarraga, J. C. Desplat, P. Bladon, Inertial effects in three-dimensional spinodal. decomposition of a symmetric binary fluid mixture: a lattice Boltzmann study, J. Fluid Mech. 440 (2001) 147–203.

[38] B. Cuenot, J. Magnaudet, B. Spennato, The effects of slightly soluble surfactants on the flow around a spherical bubble, J. Fluid Mech. 339 (1997) 25–53.

[39] G. B. McFadden, A. A. Wheeler, On the Gibbs adsorption equation and diffuse interface models, Proc. R. Soc. Lond. A 458 (2021) (2002) 1129–1149.

[40] A. K. Gunstensen, D. H. Rothman, S. Zaleski, G. Zanetti, Lattice Boltzmann model of immiscible fluids, Phys. Rev. A 43 (8) (1991) 4320–4327.

[41] X. Shan, H. Chen, Lattice Boltzmann model for simulating flows with multiple phases and components, Phys. Rev. E 47 (3) (1993) 1815–1819.

[42] M. R. Swift, W. R. Osborn, J. M. Yeomans, Lattice Boltzmann simulation of nonideal fluids, Phys. Rev. Lett. 75 (5) (1995) 830–833.

[43] X. He, S. Chen, R. Zhang, A lattice Boltzmann scheme for incompressible multiphase flow and its application in simulation of Rayleigh-Taylor instability, J. Comput. Phys. 152 (2) (1999) 642–663.

[44] S. Chen, G. D. Doolen, Lattice Boltzmann method for fluid flows, Annu. Rev. Fluid Mech. 30 (1) (1998) 329–364.

[45] R. G. M. van der Sman, Galilean invariant lattice Boltzmann scheme for natural convection on square and rectangular lattices, Phys. Rev. E 74 (2006) 026705.

[46] A. F. H. Ward, L. Tordai, Time-dependence of boundary tensions of solutions I. the role of diffusion in time-effects, J. Chem. Phys. 14 (7) (1946) 453–461.

[47] X. Li, R. Shaw, G. M. Evans, P. Stevenson, A simple numerical solution to the Ward-Tordai equation for the adsorption of non-ionic surfactants, Comput. Chem. Eng. 34 (2) (2010) 146–153.

[48] K. J. Mysels, Diffusion-controlled adsorption on a plane: Non-ideal isotherms, Colloids Surf. 16 (1) (1985) 21 – 29.

[49] Y.-C. Liao, E. I. Franses, O. A. Basaran, Computation of dynamic adsorption with adaptive integral, finite difference, and finite element methods, J. Colloid Interface Sci. 258 (2) (2003) 310 – 321.

[50] S. Succi, The Lattice Boltzmann Equation for Fluid Dynamics and Beyond, Oxford: Oxford University Press, 2001.

[51] Q. Zou, X. He, On pressure and velocity boundary conditions for the lattice Boltzmann BGK model, Phys. Fluids 9 (6) (1997) 1591–1598.

[52] Y. T. Hu, D. J. Pine, L. G. Leal, Drop deformation, breakup, and coalescence with compatibilizer, Phys. Fluids 12 (3) (2000) 484–489.

[53] S. Lyu, T. D. Jones, F. S. Bates, C. W. Macosko, Role of block copolymers on suppression of droplet coalescence, Macromolecules 35 (20) (2002) 7845–7855.

[54] Y. Yoon, A. Hsu, L. Leal, Experimental investigation of the effects of copolymer surfactants on flow-induced coalescence of drops, Phys. Fluids 19 (2) (2007) 023102.

[55] P. Yue, J. J. Feng, C. Liu, J. Shen, Diffuse-interface simulations of drop coalescence and retraction in viscoelastic fluids, J. Non-Newton. Fluid Mech. 129 (3) (2005) 163 – 176.

[56] W. Yu, C. Zhou, Coalescence of droplets in viscoelastic matrix with diffuse interface under simple shear flow, J. Polym. Sci. Part B: Polym. Phys. 45 (14) (2007) 1856–1869.